ISSN 1028-8546

Volume XX, Number 3
Section: En
November, 2014

Azerbaijan Journal of Physics

Fizika

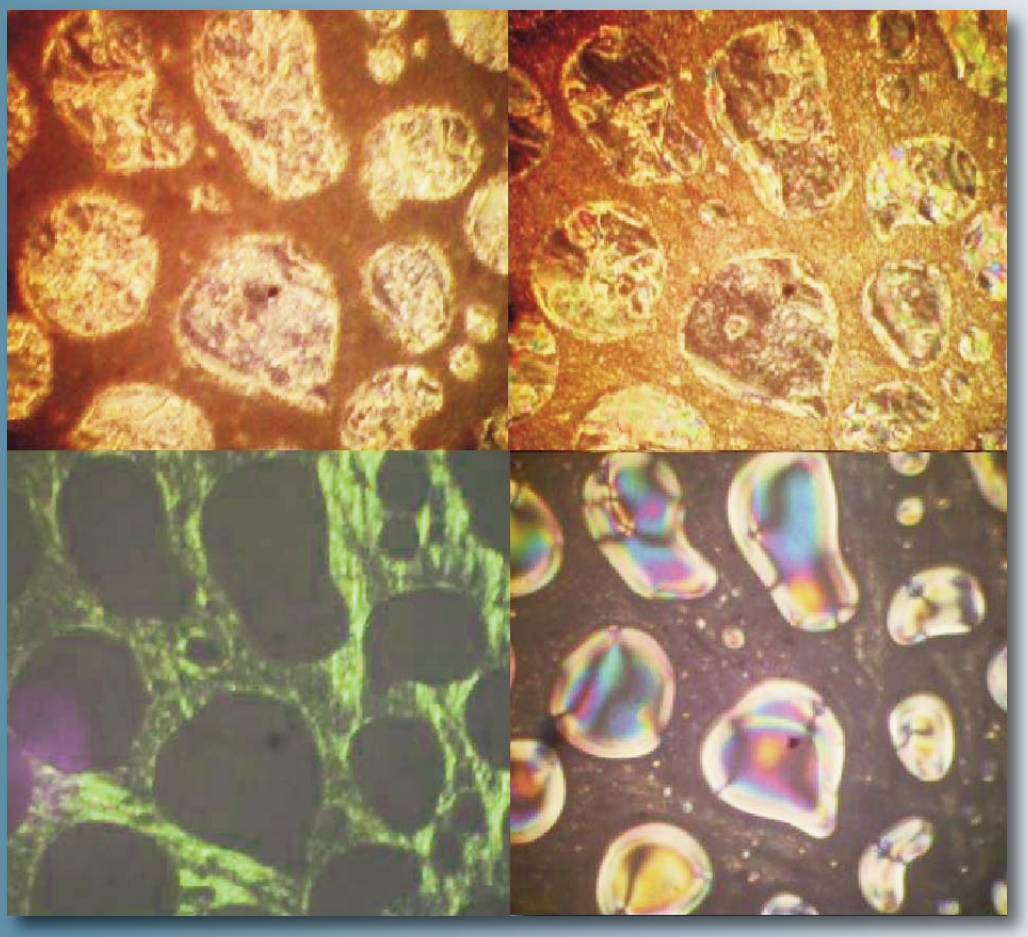

www.physics.gov.az

G.M. Abdullayev Institute of Physics
Azerbaijan National Academy of Sciences
Department of Physical, Mathematical and Technical Sciences

Published from 1995
Ministry of Press and Information
of Azerbaijan Republic,
Registration number 402, 16.04.1997

ISSN 1028-8546
vol. XX, Number 3, 2014
Series: En

Azerbaijan Journal of Physics

FIZIKA

G.M.Abdullayev Institute of Physics
Azerbaijan National Academy of Sciences
Department of Physical, Mathematical and Technical Sciences

PUBLISHING OFFICE

131 H.Javid ave, AZ-1143, Baku
ANAS, G.M.Abdullayev Institute of Physics

Tel.: (99412) 439-51-63, 439-32-23
Fax: (99412) 447-04-56
E-mail: jophphysics@gmail.com
Internet: www.physics.gov.az

It is authorized for printing:

Published at "**SƏRQ-QƏRB**"
17 Ashug Alessger str., Baku
Typographer : Aziz Gulaliyev

Sent for printing on: __.__. 201_
Printing approved on: __.__. 201_
Physical binding:_____
Number of copies:_____200
Order:_____

THE FEATURES OF THE ENERGY SPECTRUM OF ELECTRON *n*-GaAs FROM DATA ON ELECTRON TRANSPORT AT HYDROSTATIC PRESSURE

M.I. DAUNOV, U.Z. ZALIBEKOV, I.K. KAMILOV, A.Yu. MOLLAEV
Amirkhanov Institute of Physics, Dagestan Scientific Center of RAS, Makhachkala, 367003 Russian Federation
Correspondent author. E-mail: a.mollaev@mail.ru

The results on the quantitative analysis of experimental data on the baric dependences of the resistivity and Hall coefficient in *n*-GaAs at hydrostatic pressures from atmospheric up to 18 GPa are reported. A deep donor center is found. A position of its energy level relative to the Γ – valley edge of conduction band at the atmospheric pressure and its belonging to arsenic vacancies is considered.

Keywords: deep donor center, energy level, resistivity and Hall coefficient.
PACS: 71.20.Pp, 71.55.Ht.

1. The hydrostatic pressure is reckoned among the effective external influences for the research of impurity energy spectrum. An application of the hydrostatic is especially operative in detection of deep impure and deep resonance impure centers, of which energy levels are in a band continuum. Unlike the shallow impure centers keeping track of own band, with which they are genetically related, the energy of deep impure centers with respect to the absolute vacuum, according to data analysis in [1-4] and within an experimental error, remains constant at the isotropic compression of a crystalline lattice. The reason for this is that their wave functions should be plotted throughout the Brillouin zone and an influence of the hydrostatic pressure on their energy is determined by the evolution of the whole structure of energy spectrum, not just one or two nearest bands [5-7].

It is pertinent to note that specification of impure center, whether it is shallow or deep, is difficult using only results of a phenomenological description of the impure center by data on ionization energy, capture cross-section, etc. under the hydrostatic pressure [1-4]. In this regard, the investigation of the energy spectrum evolution of charge carriers in semiconductors with deep and deep resonance impure centers under the hydrostatic pressures important today, especially in well-studied materials such as GaAs.

Present work reports the quantitative analysis results of data on the baric dependence of the specific resistivity ρ and Hall coefficient R_H on atmospheric pressure up to P=18 GPa in n–GaAs under hydrostatic pressures [8, 9].

2. It is known [9, 10] that the ρ in n – GaAs sharply increases at $P>2$ GPa with a rise in a hydrostatic pressure and saturates at P = (5÷6). The Hall coefficient (R_H) weakly depends on a pressure up to *2GPa*, passes through the extremum, and is similar in a quantity at the atmospheric pressure at P = *(5÷6) GPa* (Fig.1). Such dependences of $\rho(P)$ and $R_H(P)$ are caused by a Γ-X transition in the conduction band (Fig. 1) and the percolation of electrons from Γ – valley into X-valley. The baric coefficient of a forbidden band width between the X-valley bottom and of a valance band top is negative: $\Delta=d\mathcal{E}_{gx}/dP$ = *-14 meV/GPa*. The edge of Γ-valley is higher of $\mathcal{E}_x$ more than *300 meV* at $P>6$ GPa and the electron concentration in Γ-valley $n_e \approx 0 (d\mathcal{E}_{ge}/dP$ = *94 meV /GPa*, $\mathcal{E}_{cx} - \mathcal{E}_{ce}$ = *360 meV at P=0*) [9,10]. In addition, the energy level of impure center $\mathcal{E}_{d1} = (0.15 - 1.1 \cdot 10^{-7} N_d^{1/3})$ eV [9] is found by the data on the resistivity-temperature and Hall-coefficient-temperature dependences at atmospheric pressures in volume crystals *n*–GaAs with the excess donor concentrations of $N_d = 1.8 \cdot 10^{16} cm^{-3} \div 5.5 \cdot 10^{17} cm^{-3}$

The ρ decreases in the interval $10GPa<P<18GPa$ at $P>10$ (electron concentration in Γ-valley $n_\Gamma \approx 0$) (Fig. 2) [8]. This indicates the presence of the energy level of deep donor center $\mathcal{E}_{d2}$ under a X-valley bottom of conduction band $\mathcal{E}_{cx}$, as the energy gap between it and X – valley edge ($\mathcal{E}_{cx}$ - $\mathcal{E}_{d2}$) decreases (Fig.1) and correspondingly the concentration of electrons in X-valley increases.

The quantitative analysis of $\rho(P)$ dependence at $10GPa<P<18GPa$ shows that the energy level of the deep donor is found near the Γ – valley edge at atmospheric pressure. Calculations have been made at varying a total concentration of electrons in both valleys of the conduction band $(10^{15} \div 10^{18})$ $cm^{-3}$and at taking into account the independence of deep impure center energy from the hydrostatic pressure relative to the perfect vacuum [1-4] using correlations:

$$\beta \exp \varepsilon_{d1} = \frac{1 - A}{A \exp\left[(P_1 - P_3)\Delta^* - \eta_{X3}\right] - \exp\left[(P_1 - P_2)\Delta^* - \eta_{X2}\right]} \quad (1)$$

$$A = \frac{n_{C1} - n_{C3}}{n_{C1} - n_{C2}} \cdot \frac{\exp\left[(P_1 - P_2)\Delta^* + \eta_{X1} - \eta_{X2}\right] - 1}{\exp\left[(P_1 - P_3)\Delta^* + \eta_{X1} - \eta_{X3}\right] - 1} \quad (2)$$

$$\frac{n_{C1}-n_{C3}}{n_{C1}-n_{C2}}=\frac{n_{d3}-n_{d1}}{n_{d2}-n_{d1}} \quad (2a)$$

$$n_{dj}=\frac{N_d}{1+\beta\exp(\varepsilon_{dj}-\eta_{xj})} \quad (3)$$

$$\frac{\rho}{\rho_0}=\frac{n_{\Gamma 0}}{n_\Gamma}\cdot\frac{b}{b+c} \quad (4)$$

$$\frac{R_H}{R_{H0}}=\frac{n_{\Gamma 0}}{n_\Gamma+n_X}\cdot\frac{(b^2+c)(1+c)}{(b+c)^2} \quad (5)$$

$b = \mu_e/\mu_x$, $c = n_x/n_e$. The index «0» relates a parameter to the atmospheric pressure, the indexes «1», «2», «3» relate the parameters to pressures P_1, P_2, P_3. Pressures $P_1<P_2<P_3$ $(8GPa \le P \le 18GPa)$, η_{x1}, η_{x2}, η_{x3}, Δ^* are reduced Fermy energies relative to the X–valley edge and baric coefficient Δ, β denotes the parameter of spin degeneracy, n_e, n_{e0}, n_{X1}, n_{X2}, n_{X3} and n_{d1}, n_{d2}, n_{d3} denote the concentrations of electrons in Γ– and X– valleys and in deep donor centers, N_d denotes the concentration of deep donors. It is taken the relation of mobilities $b = 20$, the effective masses of the states density electrons of Γ – and X – valleys $m_{de} = 0.072\ m_0$, $m_{dx} = 1.2\ m_0$ [9, 10].

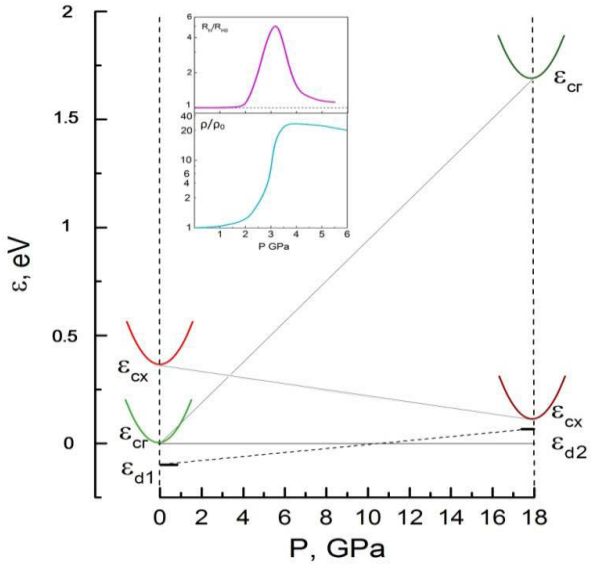

Fig.1. The dependences of Γ–valley $\mathcal{E}_{ce}$ and X – valley $\mathcal{E}_{cx}$ edges of conduction band on the hydrostatic pressure. $\mathcal{E}_{d1}$ and $\mathcal{E}_{d2}$ denote the energy of deep donor center (see in the text). Insertion exhibits the dependences of normalized specific resistivity ρ/ρ_0 and Hall coefficient R_H/R_{H0} on the hydrostatic pressure in n-GaAs [9].

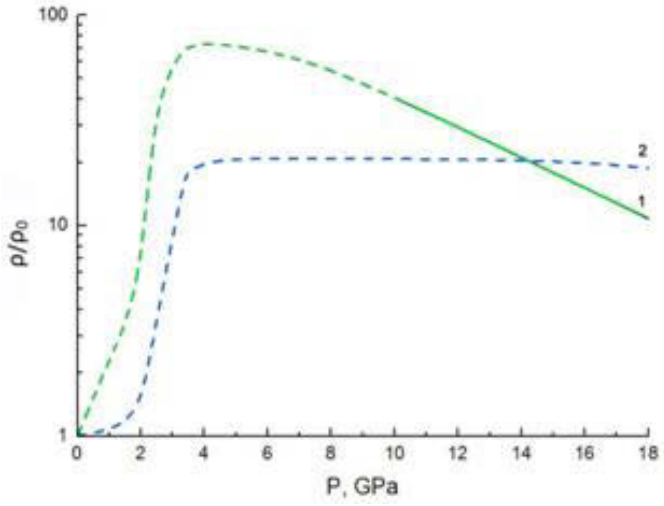

Fig.2. The dependence of normalized specific resistivity ρ/ρ_0 on pressure in *n*-GaAs: solid line denotes the experiment [8], dashed line denotes the estimation for two values of the energy of deep double donor center (see in the text).

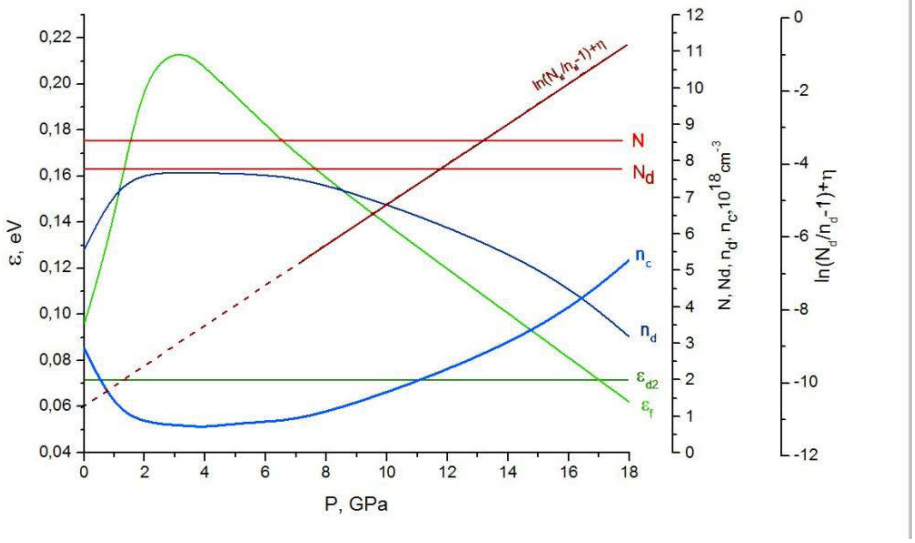

Fig. 3. Estimated baric dependences in *n*-GaAs of the Fermi energy $\mathcal{E}_F$ and the energy of deep donor center $\mathcal{E}_{d2}$ relative to Γ-valley edge at atmospheric pressure, the electron concentrations on deep donor center n_d and in conduction band $n_c = n_x+n_e$, $ln(N_d/n_d-1)+\eta$; $N = n_\Gamma+n_X+n_d$.

Fig.1-3 (curve 1) exhibit the estimations for the total concentration of electrons in Γ – and *X* – valleys of the order of $10^{18}cm^{-3}$ using correlations (1) - (5) and experimental data on *ρ(P)* dependence. By the *ρ(P)* dependence at $10\ GPa \le P \le 18\ GPa$ we derive (Fig.3)

$$\mathcal{E}_{cx} - \mathcal{E}_{d2} = (289\text{-}14P)\ meV\ (P - GPa) \qquad (6)$$

and $(\mathcal{E}_{d2} - \mathcal{E}_{c2}) = 70\ meV$ at $P=0$ (Fig.1, 3). The calculated *ρ(P), $R_H(P)$, n_Γ, n_X* dependences on the *P* estimated with account of the presence of deep donor level $\mathcal{E}_{d2}$ *(6)* (Fig.2) differ from experimental data obtained at $P<6\ GPa$ [9] (Fig.1).

Note that the presence of deep donor center in III-V and II-IV-V_2 arsenides, probably, and the electron type of conductivity in specially undoped samples is caused by the presence of arsenic vacancies [11, 12], and according to [13, 14], arsenic vacancy is a double donor and forms two energy levels relatively close disposed near the conduction band bottom at atmospheric pressure.

Indeed, at the presence of deep donor of which energy level is in the vicinity of Γ-valley edge $\mathcal{E}_{c2} - \mathcal{E}_{d1} \approx 150\ meV$ at $P=0$ the estimated *ρ(P), $R_H(P)$* dependences up to $P<6\ GPa$ agree with experimental data (Fig. 1,2), but contradict the *ρ(P)* dependence at $P>10\ GPa$ [8] (Fig.2).

So, the deep donor center $\mathcal{E}_{d2}$ found in *n*–GaAs at $10\ GPa \le P \le 18\ GPa$ is the second overlying partially settled «alternative» level of double donor – arsenic vacancy. The concentration of compensating acceptors (N_a) in considered case is $N_d<N_a<2N_d$ what is caused by a technologic prehistory.

[1] *M.I. Daunov, I.K. Kamilov and S.F. Gabibov*. (2001) *Sov. Phys. Semicond.* **35**, 58.

[2] *M.I. Daunov, I.K. Kamilov, A.B. Magomedov, S.F. Gabibov*. (2003). *Phys. Stat. Sol.* (6) **235** №2, pp. 297-301.

[3] *M.I. Daunov, I.K. Kamilov and S.F. Gabibov.* (2001). *Fiz. Tverd. Tela* **46**, 1766-1769.

[4] *I.K. Kamilov, S.F. Gabibov, M.I. Daunov, A.Yu. Mollaev*. (2011). *Phys. Techn. Polupr.*, **45**, 12, 1604-1610.

[5] *W. Paul*. Proc. 9th. Int. Conf. Semicond. (Moscow), (1968). **1**, 51.

[6] *V.A. Telejkin, K.B. Tolpigo*. Semiconductors, (1982). **16**, 1337.

[7] *In-Hwan Chor, Y.Yu. Peter*. Phys. Stat. Sol. (b) (1999). **211**, 143.

[8] *J.Z. Jiang, J.S. Olsen, L. Gerward, S. Steenstrup*. (2002). High Pressure Research, **22**, 395-398

[9] *G.D. Pitt and J. Lees*. (1970) *Phys. Rev.* (b) **2**, 10, 4144-4159

[10] Semiconductors. Group IV Elements and III-V Compounds. Ed. by o. Madelung (Springles, Berlin, 1991, Mir, Moscow. (1967).

[11] *W.D. Prochuhan*. (1974). Mater. VI Zimn. Shk. Phys. Semiconductors, 280, L.

[12] *V.N. Brudnyi*. Izv. Vyssh. Uchebn. Zaved., Fiz.,(1986). **8**, 84.

[13] *G.M. Martin, S. Makram-Ebeid*. (1986). In Deep Centers in Semiconductors, ed. By S.T. Pantelides, NY, Gordon&Breach, 399.

[14] *M. Baumler, U. Kaufmann, J. Windscheif*. (1985). Appl. Phys. Lett. **46**, 581

Recevied: 16.09.2014

MATHEMATICA IN INTEGRATION OF SELF-DUALITY EQUATIONS

M.A. MUKHTAROV
Institute of Mathematics and Mechanics
370602 Baku, F.Agaev str.9, Azerbaijan

The group element solutions of the Yang-Mill's self-duality equation are constructed by means of discrete symmetry transformations for the algebra SL(2,C) and by use of Mathematica software.

Keywords: self-duality equations, discrete symmetry transformations.
PACS: 02.30.Jr.

1. Two effective methods of integration of self-dual Yang-Mills equations (SDYM) for arbitrary semi-simple algebra has been proposed in series of papers [1-2]. Another, the discrete symmetry transformation approach has been suggested [3] that allows to generate new solutions from the old ones. This method has been applied to many cases, for instance, the exact solutions of principal chiral field problem were obtained in [4].

The discrete symmetry transformation method can be applied for deriving of the exact solutions of Yang-Mills self-duality [5] but the induction general formula has not been derived of proved up to now. The purpose of the present paper is to apply Mathematica software for obtaining of solutions of self-duality equations at any step of the reduction procedure.

2. Self-dual equations are the systems of equations for the parameters of a group element G considering as the functions of four independent arguments $z, \overline{z}, y, \overline{y}$

$$\left(G_{\overline{z}}G^{-1}\right)_z + \left(G_{\overline{y}}G^{-1}\right)_y = 0 \quad , \tag{1}$$

where $G_t=\partial_t G$.

The system of equations (1) can be partially solved

$$G_{\overline{z}}G^{-1} = f_y \quad , \quad G_{\overline{y}}G^{-1} = -f_z \quad , \tag{2}$$

where the element f takes values in the algebra of corresponding group.

System of equations on f has the following form

$$f_{z\overline{z}} + f_{y\overline{y}} + [f_z, f_y] = 0 \tag{3}$$

Following [3], for the case of a semisimple Lie algebra and for an element f being a solution of (2), the following statement takes place:

There exists such an element S taking values in a gauge group that

$$S^{-1}\frac{\partial S}{\partial y} = \frac{1}{\tilde{f}_-}\left[\frac{\partial \tilde{f}}{\partial y}, X_M\right] - \frac{\partial}{\partial \overline{z}}\frac{1}{\tilde{f}_-}X_M$$
$$S^{-1}\frac{\partial S}{\partial z} = \frac{1}{\tilde{f}_-}\left[\frac{\partial \tilde{f}}{\partial z}, X_M\right] + \frac{\partial}{\partial \overline{y}}\frac{1}{\tilde{f}_-}X_M \tag{4}$$

Here X_M is the element of the algebra corresponding to its maximal root divided by its norm, $-\tilde{f}_-$ - is the coefficient function in the decomposition of $\tilde{f}$ of the element corresponding to the minimal root of the algebra, $\tilde{f} = \sigma f \sigma^{-1}$ and where σ is an automorfism of the algebra, changing the positive and negative roots.

In the case of algebra SL(2,C) we'll consider the case of three dimensional representation of algebra and the following form of $\sigma = \begin{pmatrix} 0 & 1 \\ -1 & 0 \end{pmatrix}$.

The discrete symmetry transformation, producing new solutions from the known ones, is as follows:

$$\frac{\partial F}{\partial y} = S\frac{\partial \tilde{f}}{\partial y}S^{-1} + \frac{\partial S}{\partial \overline{z}}S^{-1} \quad , \frac{\partial F}{\partial z} = S\frac{\partial \tilde{f}}{\partial z}S^{-1} - \frac{\partial S}{\partial \overline{y}}S^{-1} \tag{5}$$

Using (2) the relations (5) can be rewritten in terms of group-valued element as

$$\left(S_n\sigma g_n\right)_{\overline{z}}\left(S_n\sigma g_n\right)^{-1} = \left(f_{n+1}\right)_y \ , \ \left(S_n\sigma g_n\right)_{\overline{y}}\left(S_n\sigma g_n\right)^{-1} = -\left(f_{n+1}\right)_z \ ,$$

where

$$\left(g_n\right)_{\overline{z}}g_n^{-1} = \left(f_n\right)_y \ , \ \left(g_n\right)_{\overline{y}}g_n^{-1} = -\left(f_n\right)_z$$

So we see that the group valued elements g_{n+1} and g_n are connected by the relation

$$g_{n+1} = S_n\sigma g_n \tag{6}$$

3. Let's represent the explicit formulae of the recurrent procedure of obtaining the group-valued element solutions of the self-duality equations in the case of SL(2,C) algebra .

As the initial solution we'll take the explicit solution f belonging to the algebra of upper triangular matrixes:

$$f = \alpha X + \tau h \tag{7}$$

The component form of self-duality equations for this case is following

$$\Box\tau = 0, \qquad \Box\alpha_i = \{\tau, \alpha\}_{y,z} \tag{8}$$

where $\Box = \frac{\partial^2}{\partial z \partial \bar{z}} + \frac{\partial^2}{\partial y \partial \bar{y}}$;

figure brackets of two functions g_1 and g_2 denotes :

$$\{g_1, g_2\}_{y,z} = \frac{\partial g_1}{\partial y}\frac{\partial g_2}{\partial z} - \frac{\partial g_2}{\partial y}\frac{\partial g_1}{\partial z}.$$

The result of integration of the system (8) can be expressed in terms of chains of solutions of the following system of linear equations

$$(\alpha^k)_{\bar{z}} - (\tau)_y \alpha^k = (\alpha^{k+1})_y$$
$$-(\alpha^k)_{\bar{y}} - (\tau)_z \alpha^k = (\alpha^{k+1})_z, \tag{9}$$

which are nothing more than Backlund transformations.

The discrete symmetry transformation allows carrying out the recurrent procedure of finding the solution of (2)

The solutions are expressed in terms of chains (9) starting from the 0-step (3).

We are using the following parameterization of the group element:

$$g_{n+1} = Exp(\alpha[n]X^+)Exp(t[n]h)Exp(\beta[n]X^-)$$

Below one can find the *Mathematica* program of the first two steps of recurrent procedure.

The *input* is written in Bold style, the results – in Normal.

```
In[1]:= X+ = {{0, 1}, {0, 0}}; X- = {{0, 1}, {0, 0}}; h = {{1, 0}, {0, -1}}; w = {{0, 1}, {-1, 0}};

        G0 = MatrixExp[n X+].MatrixExp[r h];
        S1 = MatrixExp[s[1] X+].MatrixExp[s0[1] h]; G1 = S1.w.G0;
        G1

Out[4]= {{-E^(r-s0[1]) s[1], E^(-r+s0[1]) - E^(-r-s0[1]) n s[1]}, {-E^(r-s0[1]), -E^(-r-s0[1]) n}}

In[5]:= G1 = FullSimplify[G1 /. s[1] → a[1] /. n → a[-1] /. s0[1] → Log[a[0]]]

Out[5]= {{-(E^r a[1])/a[0], (E^-r (a[0]^2 - a[-1] a[1]))/a[0]}, {-E^r/a[0], -(E^-r a[-1])/a[0]}}

In[6]:= β[1] = G1[[2, 1]]/G1[[2, 2]]; α[1] = G1[[1, 2]]/G1[[2, 2]];
        t[1] = -Log[G1[[2, 2]]];
        FullSimplify[α[1]]

Out[8]= -(a[0]^2/a[-1]) + a[1]

In[9]:= FullSimplify[t[1]]

Out[9]= -Log[-(E^-r a[-1])/a[0]]

In[10]:= β[1] = G1[[2, 1]]/G1[[2, 2]]

Out[10]= E^(2 r)/a[-1]
```

```
In[11]:= s0[2] = Log[Det[{{a[0], a[1]}, {a[1], a[2]}}] / a[0]];

         s[2] = (a[0] Det[{{a[0], a[2]}, {a[1], a[3]}}] - a[1] Det[{{a[0], a[1]}, {a[1], a[2]}}]) / a[0]^2;

         S2 = MatrixExp[s[2] X^].MatrixExp[s0[2] h];
         G2 = S2 . w . G1;
         β[2] = G2[[2, 1]] / G2[[2, 2]];
         α[2] = G2[[1, 2]] / G2[[2, 2]];
         t[2] = -Log[G2[[2, 2]]];
         FullSimplify[β[2]]
         Null

Out[18]=  e^(2 r) a[1] / (-a[0]^2 + a[-1] a[1])

In[20]:= FullSimplify[t[2]]

Out[20]= -Log[e^(-r) (a[0]^2 - a[-1] a[1]) / (a[1]^2 - a[0] a[2])]

In[21]:= FullSimplify[α[2]]

Out[21]= (a[1]^3 - 2 a[0] a[1] a[2] + a[-1] a[2]^2) / (a[0]^2 - a[-1] a[1]) + a[3]
```

The last expression is nothing more than

$$\alpha[2]=\frac{Det\begin{pmatrix} a[-1] & a[0] & a[1] \\ a[0] & a[1] & a[2] \\ a[1] & a[2] & a[3] \end{pmatrix}}{Det\begin{pmatrix} a[-1] & a[0] \\ a[0] & a[1] \end{pmatrix}}$$

Using the expressions for the group-value elements and the relations (1), one can easily come to final expressions for the algebraic solutions, presented in [1]:

$$f_n^- = \frac{Det_{n-1}(a)}{Det_n(a)}, f_n^0 = \tau + \frac{\tilde{D}_n(a)}{Det_n(a)}, f_n^+ = \frac{Det_{n+1}(a)}{Det_n(a)},$$

where $Det_n(a)$ are the minors of order n of the following matrix:

$$\alpha = \begin{pmatrix} a[0] & a[1] & a[2] & \dots \\ a[1] & a[2] & a[3] & \dots \\ a[2] & a[3] & a[4] & \dots \\ \dots\dots & \dots\dots & \dots\dots & \dots \\ \dots\dots & \dots\dots & \dots\dots & \dots \end{pmatrix}$$

Here $\tilde{D}_n(a)$ denotes that in the last row of the corresponding matrix the indices of $a[i]$ have been increased by one.

[1] *M.F.Atiyah,N.J.Hitchin,V.G. Drinfeld and Yu.I. Manin*. Phys. Lett. A65, 1978, 2.

[2] *A.N.Leznov and M.A.Mukhtarov*. J.Math. Phys. 28 (11), 1987, 2574; Prepr.IHEP 87-90, 1987; Prepr. ICTP 163, Trieste, Italy,1990; J.Sov. Lazer Research, 13 (4), 284, 1992.

[3] *A.N. Leznov*. IHEP preprint-92/87,1990.

[4] *A.N.Leznov,M.A.Mukhtarov and W.J.Zakrzewski*. Tr.J.of Physics 19, 416, 1995.

[5] *M.A. Mukhtarov*. Fizika 5, 4, 1999.

Recevied: 21.06.14

ELECTRO-OPTICS OF NOVEL POLYMER-LIQUID CRYSTALLINE COMPOSITES

T.D. IBRAGIMOV [a], G.M. BAYRAMOV[a,b], A.R. IMAMALIEV[a]

[a]*Institute of Physics of National Academy of Sciences. 33 H.Javid Avenue, AZ1143. Baku, Azerbaijan.*
E-mail: tdibragimov@mail.ru

[b]*Baku State University. 23 Z.Khalilov street, AZ1148. Baku, Azerbaijan*[b]

The polymer network liquid crystals based on the liquid crystals H37 and 5CB with polymethylvinilpirydine (PMVP) and polyethyleneglycol (PEG) have been developed. Mesogene substance heptyoxibenzoic acid (HOBA) is served for stabilization of obtaining composites. Kinetics of network formation is investigated by methods of polarization microscopy and integrated small-angle scattering. It is shown that gel-like states of the composite H-37 + PMVP + HOBA and 5CB+PEG+HOBA are formed at polymer concentration above 7 % and 9 %, correspondingly.

The basic electro-optic parameters of the obtained composites are determined at room temperature. Experimental results are explained by phase separation of the system, diminution of a working area of electro-optical effects and influence of areas with the high polymer concentration on areas with their low concentration.

Keyword: polymer network liquid crystal, small-angle scattering, phase transition, the threshold voltage, electrohydrodynamic instability
PACS: 42.70.Df; 47.20.Cn; 47.32.Cd; 61.30.Gd.

1. INTRODUCTION

One of ways of improvement of electro-optical parameters and creation of more convenient methods of using electro-optical effects in liquid crystals (LC) is development of hybrid systems, in particular, polymer-liquid crystal composites. These composites are subdivided into two basic types depending on polymer concentration. The first of them is formed at the high polymer concentration and called polymer dispersed liquid crystal [1]. It composes of micro-sized LC droplets embedded in a polymer matrix.

At application of electric field to the system, there is a reorientation of a primary direction (director) of LC molecules. Owing to this factor, the similar composites are used as a light shutter, a modulator, a flexible display. Moreover, a compact temperature indicator could be developed, applying thermochromic cholesteric LC which reflects certain color at specific temperatures [2].

At low polymer concentration, the system called polymer network liquid crystal is formed [3]. At this case, all basic electro-optical effects in liquid crystals are also characteristic for this system but with the changed parameters and appearance of new effects.

For preparation of polymer network liquid crystal, phase separation is induced by polymerization of monomer, solvent application or thermal method. Heretofore, the limited number of such composites is developed which have been studied by various methods [3-8].

Therefore, a search of new composites with the improved electro-optical parameters is an actual problem and has practical interest.

The present work is devoted to the kinetics of formation of polymer network liquid crystals based on the liquid crystals H37 and 5CB, dispersed by polymethylvinylpyridine and poly(ethyleneglycol), and determination of its basic electro-optic parameters.

2. EXPERIMENTAL

We used liquid crystalline mixture H 37 consisting of 4-methoxybenzylidene-4'-butylaniline and 4-ethoxybenzylidene-4'-butylaniline with molar ratio of 1:1 and liquid crystal 4-pentylcyano-4'-biphenyl (5CB) were used as the matrixes. The first mixture has negative dielectric anisotropy - 0.6 and the range of the nematic phase between -10 ^{o}C and 61 ^{o}C while the second has positive dielectric anisotropy +11.7 and the nematic state between 21 ^{o}C and 35.2 ^{o}C.

The powder of poly (2-methyl-5-vinylpyridine) (PMVP) with average sizes of 2 mμ, having molar mass of 30000 and cure temperature about 130^{o}C and also polymer poly(ethyleneglycol) (PEG*)* with 1 μm sizes, having molar mass of 30000 with cure temperature 54°C were used as fillers.

Investigation was carried out in electro-optic cells having a sandwich structure and consisted of two plane-parallel glass plates whose inner surfaces were coated with thin transparent and conductive layer ITO (Indium-Tin-Oxide). Planar orientation of molecules was reached by coating of inner substrate surfaces with rubbed polyimide layers. For obtaining of homeotropic orientation of LC molecules, we used the surfactants (soup solution or lecithin). The thickness of the cell was 20 μm. The mixture was filled into the cell by capillary action at temperature 140^{o}C. Mesogene substance 4-n-heptyoxibenzoic acid (HOBA) was served for stabilization of obtaining composites.

Identification of the phase state and a study of electro-optic properties of the composites have been carried out by the equipment assembled on the base of polarization microscope POLAM 111. At this case, a quasi-static saw-tooth voltage was applied to the electro-optic cell. Latter with the mixture was kept in the special heater in which the copper-constantan thermocouple was used for temperature

measurements. Temperature stabilization and its determination accuracy were 0.1°C.

In order to measure the integrated flux of scattered radiation from the cell with composite, a setup assembled on the base of He-Ne laser LG-75 (wavelength 632.8 nm and power 25 mW) and optical bench OS-5 was used. At this case, the small septum was arranged in front of the detector for an exception of radiation passing through the sample from scattered light. The latter was detected between 0.5 and 4.0 angular degrees.

3. RESULTS AND DISCUSSION

The mechanical mixture of polymer and liquid crystal is heated above a cure temperature of polymer and kept at this temperature for 1 hour. Then it is slowly cooled to room temperature. Observation has shown that H-37 + PMVP + HOBA and 5CB + PEG + HOVA at weight concentrations of polymer above 7 % and 9 %, respectively, a gel-like state of the composites is formed at which their viscosity sharply increases. A change of the texture of the composite H-37 + PMVP + HOBA (87 % + 12 % + 1 %) in the cooling process is shown in Fig. 1.

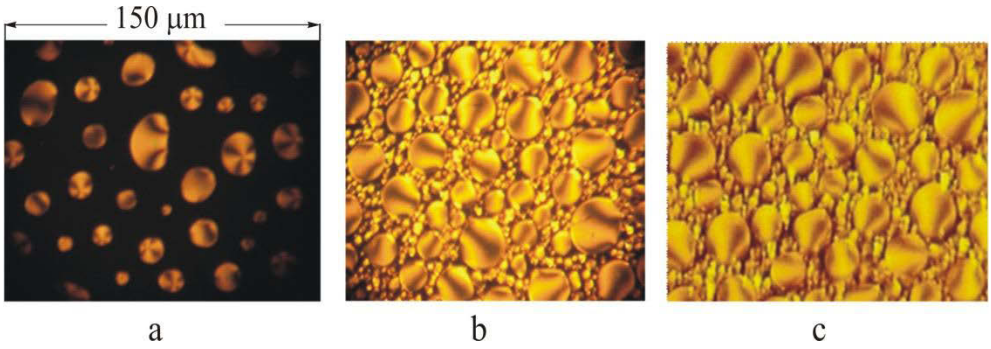

Fig.1. Network formation of the composite H-37 + PMVP + HOBA (87%+12%+1%) from the isotropic phase at cooling rate of 1°C/min: (a) T=48.4 °C, (b) T=40.5°C, (c) T=22.5°C.

One can see light areas corresponding to an anisotropic state of the composite are observed only below temperature 49 °C while the isotropic - nematic transition of the pure LC occurs at 61 °C. In addition, a dramatic increase of an intensity of integral small-angle scattering light corresponding to this temperature is observed (Fig. 2).

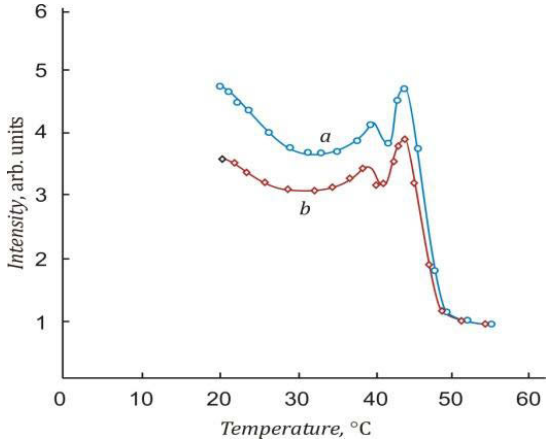

Fig.2. Temperature dependence of integrated intensity of small-angle scattering of laser radiation from H-37 + PMVP + HOBA (87%+12%+1%) in the cooling regime at various cooling rates: a - 2 °C/min; b- 1 °C/min.

Apparently, it connects with a nucleation of new phase. The scattered radiation intensity decreases at decreasing of the cooling rate, connecting with more consistency of the structure. According to [8], similar mixtures are separated on polymer - rich and polymer - poor phases at its slow cooling below some temperature T_c. Such separation corresponds to optimum thermodynamic balance of the system. An isotropic-nematic transition takes place in the first phase earlier than in the second. Actually, an intensity of integrated small-angle scattering from H-37 + PMVP + HOBA has a local maximum about temperature 41°C which can be connected with transition of the second phase with the more polymer concentration to a mesogene state. Observation under the polarization microscope also has confirmed an origin of the small round areas surrounding large drop-shaped areas. Moreover, there are accurate boundaries between them. Local mechanical impact has shown that these areas have different viscosity: the large areas have less viscosity than small ones. At decreasing temperature, there is penetration of LC molecules from small areas to the large drops increasing in dimensions. At this case, concentration of polymer in small areas increases, forming a uniform network which surrounds large drops. They have sizes of 10- □□30 μm. Small round areas do not react to an applied field up to 30 V while the large drops change a texture at application of electric field that is they appear themselves as working areas of electro-optical effects. It is necessary to note that the scattered radiation intensity decreases at reduction of the cooling rate. This fact is connected, apparently, to more uniform distribution of coexistent phases.

A change of the texture of the composite 5CB+PEG+HOBA (85% +13 % +2%) at cooling process is shown in Fig.3.

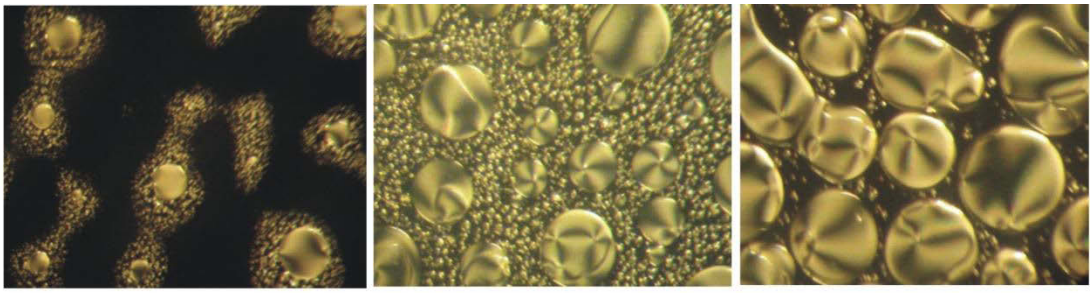

Fig.3. Texture changes of the composite 5CB+PEG+HOBA (85%+13%+2%) at cooling rate of 1 °C/ min: (a) T= 35.5 °C, (b) T= 33.6 °C, (c) T= 25.5 °C.

Here, an anisotropic state is observed below 36°C. In order to describe the changes of this composite, the measurements of the integrated intensity of small-angle scattering have also been carried out. The temperature dependences of small-angle scattering intensity in the cooling regime are shown in Fig.4.

As we can see, the strong scattering connected with formation of polymer solid areas in the isotropic phase of 5CB is appeared near the cure temperature of the polymer. A second maximum of scattering intensity takes place at temperature 36°C corresponding to the isotropic-nematic transition of the pure LC. Here, the scattered radiation intensity also decreases at decreasing of the cooling rate, connecting with stabilization of the structure. It is note that the composite 5CB+PEG+HOBA is no thermoreversible, that is the initial structure is not restored at heating and subsequent cooling. At heating the LC areas transform to the isotropic state while polymeric walls remain without changes (Fig.5).

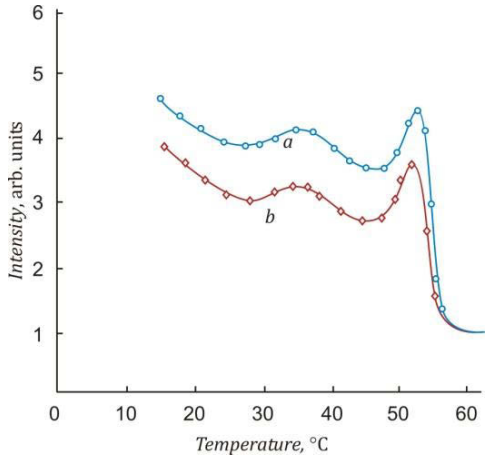

*Fig.4.*Temperature dependence of integrated intensity of small-angle scattering of laser radiation in 5CB+PEG+HOBA (84%+12%+4%) at different cooling rates:(a) 2°C/hour, (b) 1 °C/hour.

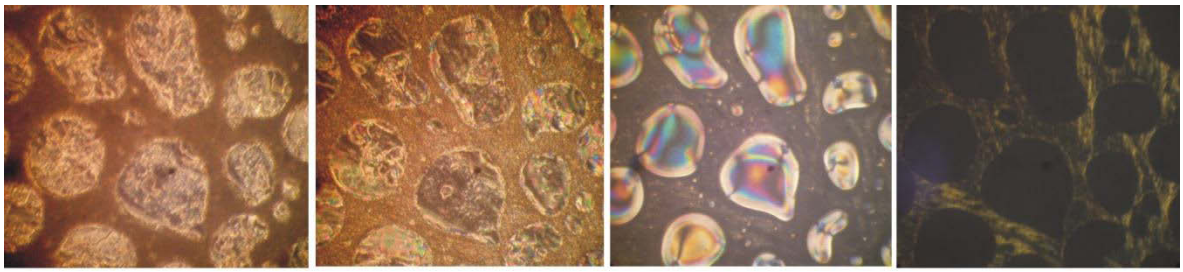

Fig.5. Texture changes of the composite 5CB+PEG+HOBA (85%+13%+2%) at heating rate of 1 °C/ min: (a) T= 35.5 °C, (b) T= 33.6 °C, (c) T= 25.5 °C.

Measurements of threshold voltages of the homeotropic-planar transition and the electrohydrodynamic instability of H-37 + PMVP + HOBA (87 % + 12 % + 1 %) show that their magnitude increases for the composite in comparison with the pure LC from 1.9 V to 8.7 V and from 8.5V to 9.4 V, correspondingly. A voltage of the planar-homeotropic transition equals to 2.4 V for 5CB+PEG+HOBA (85% +13 % +2%) and 0.9 V for pure 5CB, and electrohydrodynamic instability occurs at the same voltage 7.5 V for the composite and pure LC. These facts may be explained as follows. Frederick effect arises at excess of an energy density of applied electric field w_f over

a density of elastic energy w_e of LC medium. An energy density of electric field is described by the following expression [9]:

$$w_f = 1/2\ (\Delta\varepsilon\varepsilon_o U^2/d^2).$$

Here, $\Delta\varepsilon$ is dielectric anisotropy, ε_o is electric constant, U is electric voltage, and d is thickness of the cell.

For the pure LC the density of elastic energy is defined by [9]:

$$w_e = 1/2\ (K_{33}\pi^2/d^2),$$

where K_{33} is the bend elastic constant.

As a result, we obtain the expression for the threshold voltage of a pure LC:

$$U_{th} = \pi\ (K_{33}/\Delta\varepsilon\varepsilon_0)^{1/2}.$$

A working area (the liquid crystal with the low polymer concentration) of the composite is located within more limited volume. As a rough approximation, these areas can be accepted as cylinders with height d and radius R. In order to turn the director in these areas, a minimum of the density of elastic energy is equal:

$$w_e = 1/2(K_{33}\pi^2/d^2) + 1/2\ (K_{11}\pi^2/d^2),$$

where K_{11} is an elastic constant of splay deformation of the director. The addend in the density of elastic energy is caused by robust coupling of LC molecules with side walls. Whereas R has an order of the cell thickness, the contribution of the second addend in the density of elastic energy is essential (K_{11} is greater by several fold than K_{33}). Besides, the homeotropic - planar and planar – homeotropic transitions are accompanied by formation of strength declination +1/2 [10]. An increase of elastic energy density and formation of declinations are the reason of a growth of the threshold voltages of Frederick transition and electrohydrodynamic instability.

Dependences of a rise time of electro-optical effects on voltage for H-37 + PMVP + HOBA (87% + 12% + 1%) at which the region of low voltages corresponds to the homeotropic-planar transition process, and the high voltage region does to the electrohydrodynamic instability are resulted in Fig.6. Apparently, a rise time decreases monotonically with increasing of voltage. At this case, the curve corresponding to the composite is shifted to the high voltage region. Obtained experimental results are good agree with known expressions for a rise time at both homeotropic-planar transition and electrohydrodynamic instability. Really, dependences of a rise time of the homeotropic-planar transition and the electrohydrodynamic instability on voltage for a pure LC are defined by formulae [10]:

$t = 4\pi\gamma_1 d^2/\varepsilon_o\Delta\varepsilon(U^2\text{-}U_{th}^2)$ and $t = \beta\eta d^2/(U^2\text{-}U_{th}^2)$, respectively. Here, γ_1- rotational viscosity (Lesley coefficient), η is translational viscosity of LC, β is factor depending on material parameters of LC.

At a first approximation, these expressions are true for LC with low polymer concentration. Large magnitude of a rise time of the composite in comparison with corresponding magnitude for pure LC connects with an increase of the LC viscosity at addition of polymer. An existence of long chains of polymer macromolecules in LC obstructs both rotational and translational motions of LC molecules.

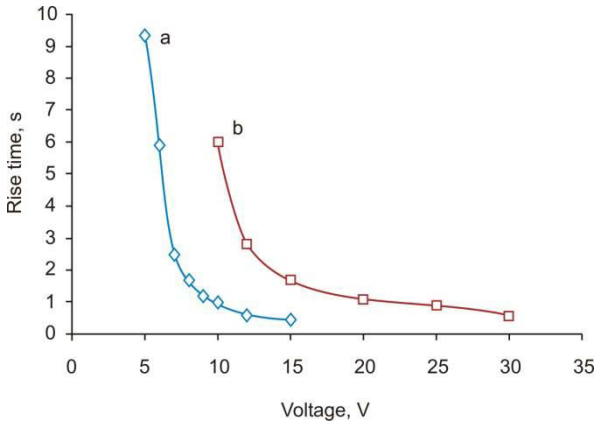

Fig.6. Dependence of a rise time of an electro-optic effect on quasi-static voltage: (a) pure H37, (b) H-37+PMVP+HOBA (87%+12%+1%).

Dependence of a decay time on applied voltage for both pure LC and the composite is presented in Fig.7. As

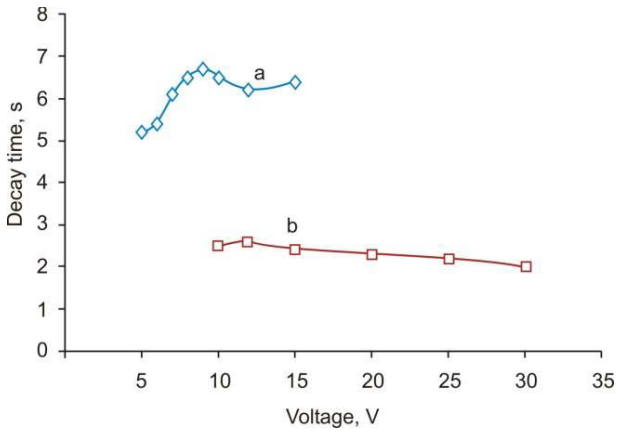

Fig.7. Dependence of a decay time of an electro-optic effect on quasi-static voltage: (a) pure H3, (b) H-37+PMVP+HOBA (87%+12%+1%).

seen, corresponding dependence for the pure LC has a maximum of 9V at which relaxation of electro-optic response essentially changes and corresponds to the transition from field regime to current one. A decay time is less for the composite than for the pure LC at all applied voltages. It is explained by following way. According to [9], a decay time at the regime of homeotropic-planar transition: $t=\gamma_1 d^2/\pi^2 K_{33}$ and at the regime of electrohydrodynamic instability: $t = \eta d^2/\pi^2 K_{33}$. Namely, a decay time is directly proportional to visco-elastic ratio γ_1/K_{33} or η/K_{33}. It can be assumed that a bend elastic constant of the composite increases more than its viscosity by addition of polymer. Possibly, it is connected with presence of long polymer chains. Additionally, the side walls of working areas exert strong impact on a decay time because of its stimulation for relaxation of the director at cancellation of electric field action.

As distinguished from a rise time characteristic of the composite H-37 + PMVP + HOBA (87 % + 12 % + 1 %), a rise time of the composite 5CB + PEG + HOVA (85% + 13 % +2%) shows anomalous behavior (Fig.8): it increases as field well as current modes at voltage increasing.

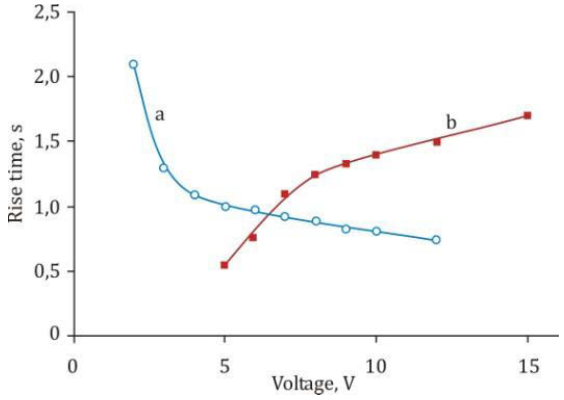

Fig.8. Dependence of a rise time of an electro-optic effect on quasi-static voltage: (a) pure 5CB, (b) 5CB+PEG+HOBA (85%+13%+2%).

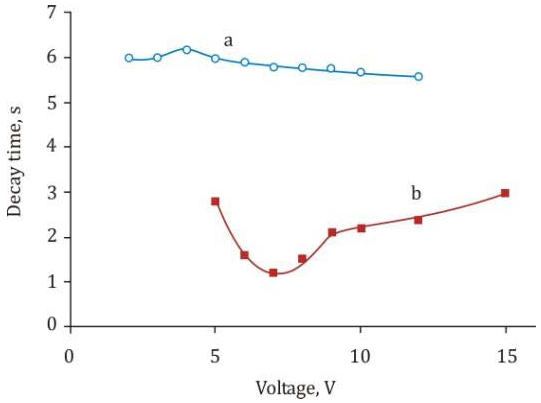

Fig.9. Dependence of a decay time of an electro-optic effect on quasi-static voltage: (a) pure 5CB, (b) 5CB+PEG+HOBA (85%+13%+2%).

A decay time also unusually behaves (Fig.9). It has a minimum at 7V which connects with the transition from field to current modes.

Apparently, such abnormal dependence of time characteristics is connected with no thermo-reversibility of the structure at heating process and incompleteness of the transition to planar state of LC molecules. For this reason, the simple model of a composite with different polymer concentration does not describe peculiarities of the threshold voltages and time characteristics.

We also note that a presence of the network gives rise to reduction of the contrast ratio owing to light scattering on this structure.

4. CONCLUSIONS

It is shown that gel-like state of the composite H-37 + PMVP + HOBA is formed at polymer concentration above 7% while the composite 5CB + PEG + HOVA passes to such state at 9 % polymer concentration. At slow cooling, the system separates into a liquid crystal – rich phase and a liquid crystal-poor phase. At this case, transition of these phases of the H-37 + PMVP + HOBA (87% + 12% + 1%) composite to an anisotropic state occurs at 49°C and и 41°C, accordingly, while the composite 5CB+PEG+HOBA (85% +13 % +2%) passes to anisotropic state at 36°C corresponding to the isotropic-nematic transition of pure 5CB.

It is shown that threshold voltages increase and, accordingly, there is a shift of voltage dependence of rise time. The contrast ratio worsens while decay time improves in comparison with the pure liquid crystal at all applied voltage. Experimental results are explained by phase separation of the system, reduction of a working area of electro-optical effect and influence of areas with the large polymer concentration on areas with their concentration.

Acknowledgements

The work has been supported by Scientific and Technology Center in Ukraine (grant no 5821).

[1] *G.P. Crawford, J.W. Doane, and S. Zumer*. Polymer Dispersed Liquid Crystals: Nematic droplets and related systems, in: Handbook of Liquid Crystal Research (edited by PJ. Collings and J.S. Patel), Oxford University Press, Oxford, 1997, pp.121-158.

[2] *S. Bronnikov, S. Kostromin, V. Zuev*. Polymer-Dispersed Liquid Crystals: Progress in Preparation, Investigation, and Application, Journal of Macromolecular Science, Part B: Physics 52 (2013) 1718-1735.

[3] *Y.K. Fung, D.-K. Yang, S. Ying, L.-C. Chien, S. Zumer, and J.W. Doane*. Polymer networks formed in liquid crystals, Liq. Cryst. 15 (1996) 797-801.

[4] *Y.K. Fung, A. Borstnik, S. Zumer, D. K. Yang, and J.W. Doane*. Pretransitional nematic ordering in liquid crystals with dispersed polymer networks, Phys. Rev. 55 (1997) 1637-1645.

[5] *A. Jakli, L. Bata, K. Fodor-Csorba, L.I. Rosta and L. Noirez*. Structure of polymer networks dispersed in liquid crystals: small angle neutron scattering study, Liq. Cryst., 17 (1994) , 227-234.

[6] *G.P. Crawford, A. Scharkowski, Y.K. Fung, J.W. Doane, and S. Zumer,* Internal surface, orientational order, and distribution of a polymer network in a liquid crystal matrix, Phys. Rev. E 52 (1995) R1273-R1276.

[7] *A. Jakli, D.R. Kim, L.-C. Chien, and A. Saupe*. Effect of a polymer network on the alignment and the rotational viscosity of a nematic liquid crystal, Appl. Phys. 72, (1992) 3161-3164.

[8] *P.S. Drzaic, Liquid Crystal Dispersions.* World Scientific Publishing Co.Ptc.Ltd, Singapore, 1995, p.p. 75-81.

[9] *S.V. Pasechnik, V.G. Chigrinov, D.V. Shmeliova* – Liquid crystals: Viscous and Elastic Properties, Wiley-VHC Verlag GmbH & Co., Heppenheim, 2009, pp. 179-186.

[10] *L.M. Blinov*. Structure and Properties of liquid Crystals, Springer: Dordrecht-Heidelberg-London-New York, 2011, pp.209-340.

Recevied: 04.06.2014

LUMINESCENCE PROPERTIES OF $Ca(Al_xGa_{1-x})_2S_4$ COMPOUND

B.G. TAGIYEV, S.A. ABUSHOV, E.G. ASADOV
Institute of Physics of Azerbaijan National Academy of Sciences
AZ-1143, Baku, G.Javid ave., 33
e-mail:elsenesedov@gmail.com

The excitation and radiation photoluminescence spectra (PhL) of $Ca(Al_xGa_{1-x})_2S_4:Eu^{2+}$ (x=0,1; 0,2) crystals are investigated. The radiation spectrum caused by $4f^65d\rightarrow4f^7(^8S_{7/2})$ of transitions Eu^{2+} ion presents itself the wide band with maximum at 2.25eV. The concentration change (from 5% up to 7%) of Eu^{2+} ions increases PhL intensity value almost in three times. The zero phonon line energy (E_0=2,39eV) and Stokes shift are defined from PhL spectra. The radiation band maximum shifts to the short-wave side with the increase of aluminum content.

Keywords: solid solutions, radiation spectrum, excitation, Eu^{2+} ion.
PACS: 76.30.,78.55.,78.60.

INTRODUCTION

Nowadays the study of inorganic materials is the modern scientific-technical direction combining the complex problem of task series on quantum electronics, spectroscopy, crystallography and chemical technology. The activated crystals with impurity of rareearth ions (REI) are its main objects. The production of high-production devices for visualization and lightening which are able to compete with traditional systems, requires the obtaining of luminophors with specific properties. This necessity is caused to the development of new material obtaining or optimization of already existing luminophors.

The luminescence, radiation kinetics and radiation thermal damping in single- and polycrystals $CaGa_2S_4:Eu^{2+}$ are investigated in work [1]. The luminescent properties are studied by excitation wavelengths 420 and 337,1nm. Photoluminescence properties of $BaAl_2S_4:Eu^{2+}$ crystals are investigated on spectra of diffuse reflection, excitation and radiation [2]. Such parameters as crystal field force, Stokes shift and activization energy are defined. The enission properties of isostructural crystals $BaAl_2S_4:Eu^{2+}$ are also analyzed in the given work and it is shown that thin films on the base of $BaAl_2S_4$:Eu polycrystal can be applied as electro-luminescent cells of high radiation property of water radiation. The photoluminescence spectra of $BaAl_2S_4$:Eu crystal is investigated at λ_{ex}=325nm and 300 and 80K temperatures [3]. The investigation results of MS-Al_2S_3 (M=Ca,Sr,Ba) system photoluminescence properties activated by Eu ions ($CaAl_2S_4$:Eu, $SrGa_2S_4$:Eu, $BaGa_2S_4$:Eu) are presented in [4-6].

Nowadays the luminophors II-$(M_xM_{x-1})_2VI_4$:REI (II-Ca,Ba,Sr; M-Ga; M^1- Al, VI–S,Se) attract the investigators' attention as they have the qualities required for new technologies of planar screens and inorganic screens of electro-luminescent devices including the color TV sets and light sources.

The alkali-earth chalcogenide semiconductors of II-$(M_xM_{x-1})_2VI_4$: REI (II-Ca,Ba, Sr; M-Ga; M^1- Al, VI–S,Se) types activated by rareearth elements are the more perspective ones in this aspect.

The synthesis, roentgenophase analysis and investigation of radiation properties of $Ca(Al_xGa_{1-x})_2S_4$ compounds are carried out in this work.

EXPERIMENT TECHNIQUE

The GaS compound synthesis is carried out in quartz reactor by interaction of thin-dispersed powder of calcium carbonate ($CaCo_3$) with hydrogen sulphide (H_2S) and carbon sulphide (CS_2) in Ar inert gas atmosphere. The feed rate of inert gas is 2-2,5l/h. The hydrogen sulfide and carbon sulfide form because of decomposition of dehydrated thiocyanic ammonium (NH_4CNS) in generator of gases-reagents at temperature 250^0C. The synthesis temperature is 720^0-770^0C, duration is 24 hour and temperature is controlled with the help of chromel-alumel thermocouple. The synthsis is carried out by following reactions :

$$CaCO_3 + H_2S \rightarrow CaS + H_2O + CO_2 \quad (1)$$
$$CaCO_3 + CS_2 \rightarrow CaS + CO_2 + COS \quad (2)$$

Al_2S_3 and Ga_2S_3 compounds are synthesized by melting from Ga elements of B-3(99,999%) mark, S elements of B4 (99,9999%) mark and Al elements taken in stoichiometric ratios in quartz ampoules evacuated up to 10^{-4} millimeter of mercury by following reactions:

$$2Ga + 3S \xrightarrow{1150\ ^\circ C} Ga_2S_3 \quad (3)$$
$$2Al + 3S \xrightarrow{1200\ ^\circ C} Al_2S_3 \quad (4)$$

$Ca(Al_xGa_{1-x})_2S_4$ compound is synthesized by method of solid-phase reactions from powder components GaS, Al_2S_3 and Ga_2S_3 taken in stoichiometric ratios in graphitized quartz ampoules evacuated up to 10^{-4} millimeter of mercury by reaction:

$$CaS + x(Al_2S_3) + (1-x)(Ga_2S_3) \xrightarrow{1100\ ^\circ C} Ca(Al_xGa_{1-x})_2S_4 \quad (5)$$

The activation of europium ions is carried out by introduction of EuF_3 into blend.

ROENTGENOPHASE ANALYSIS

The samples synthesized by us are examined by roentgenodiffractometrical investigations for carrying out of roentgenophase analysis.

The roentgen-diffractogram is taken on roentgen-diffractometer D8 Advance (Bruker). The analysis of roentgen diffraction of $Ca(Al_xGa_{1-x})_2S_4$ compound shows that they have the orthorhombic structure with simultaneous presence of twinning and superstructure

with space group $D_{2h}^{24} - Fddd$ (fig.1). The calcium ions are in two differnt crystal positions (Eu^{2+}-r=1.25Å, Ca^{2+}- r=1.12Å). As rareearth activators exchange especially these cations so they should be in two different positions in the given matrix.

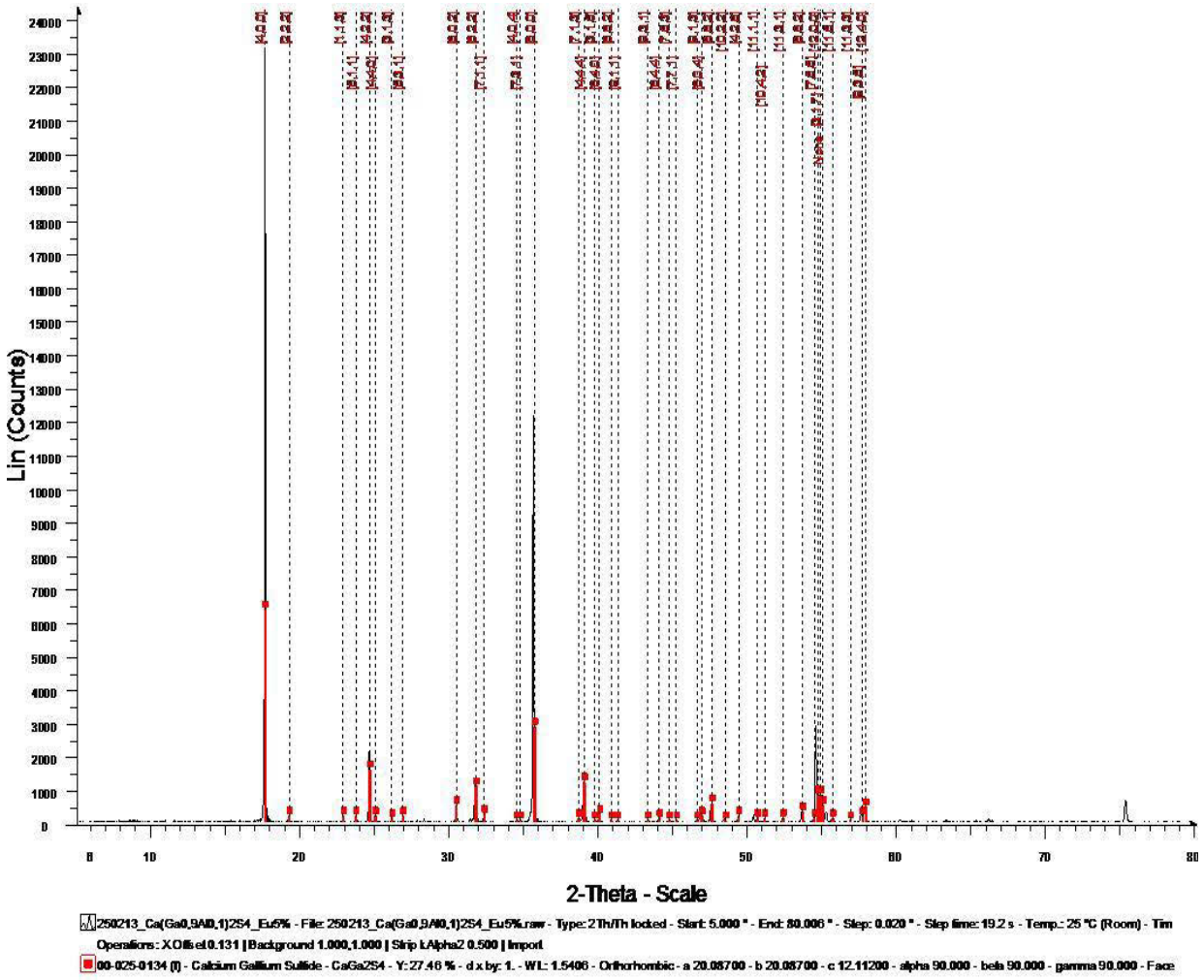

Fig1. Diffractogram of $Ca(Al_{0,1}Ga_{0,9})_2S_4:Eu^{2+}$ compound.

RESULTS AND THEIR DISCUSSION

PhL excitation and radiation spectra of $Ca(Al_xGa_{1-x})_2S_4:Eu^{2+}$ crystal are presented on fig.2. PhL excitation spectrum of $Ca(Al_xGa_{1-x})_2S_4:Eu^{2+}$ presents itself the wide band which overlaps with the radiation spectrum in wide interval (480-562 nm) of visible region (fig.2). The observable excitation spectrum one can explain by of Eu^{2+} ion absorption. $Ca(Al_xGa_{1-x})_2S_4:Eu^{2+}$ luminophor energy position of radiation spectrum maximum doesn't depend on wavelength of external excitation radiation at excitations on different wavelengths 340, 408 and 480nm. The excitation spectrum consists on short-wave 3.64 eV (340 nm), 3.03 eV (408 nm) and long-wave 2.56eV (480 nm) peaks. One can consider that if the absorption takes place on Eu^{2+} ions ($4f^7 4f^6 5d$) (see the insertion on fig.2) then it is carried out by means of matrix of luminescent substance [7] in short-wave region [7].

The radiation spectrum presents itself the band with maximum at 2.25eV and half-width 0.22eV at 300K (fig.3). The energy of zero phonon line (E_0= 2,39eV) and Stokes shift (ΔS=0,32eV) are obtained by point of intersection of PhL and PhL excitation spectra. Moreover, the transition takes place from lower excitation level $4f^6 5d$ to the ground one $4f^7$ ($^8S_{7/2}$). PhL intensity increases almost in three times with the increase of ion concentration Eu^{2+} (from 5% up to 7%). PhL spectra $Ca(Al_xGa_{1-x})_2S_4$ at x=0,1 and x=0,2 values are shown on fig.4.As it is seen from the figure, the shift of radiation band maximum into short-wave side and increase of total radiation band half-widths takes place at increase of *x* value.

The spectrum position shift to the short-wave region with x increase can be explained by increase of lattice parameters, consequently, by decrease of crystal field influence on activator Eu^{2+} [8,9]. The increase of PhL band half-width is probably connected with amplification of electron-phonon interaction in $Ca(Al_xGa_{1-x})_2S_4$ solid solutions.

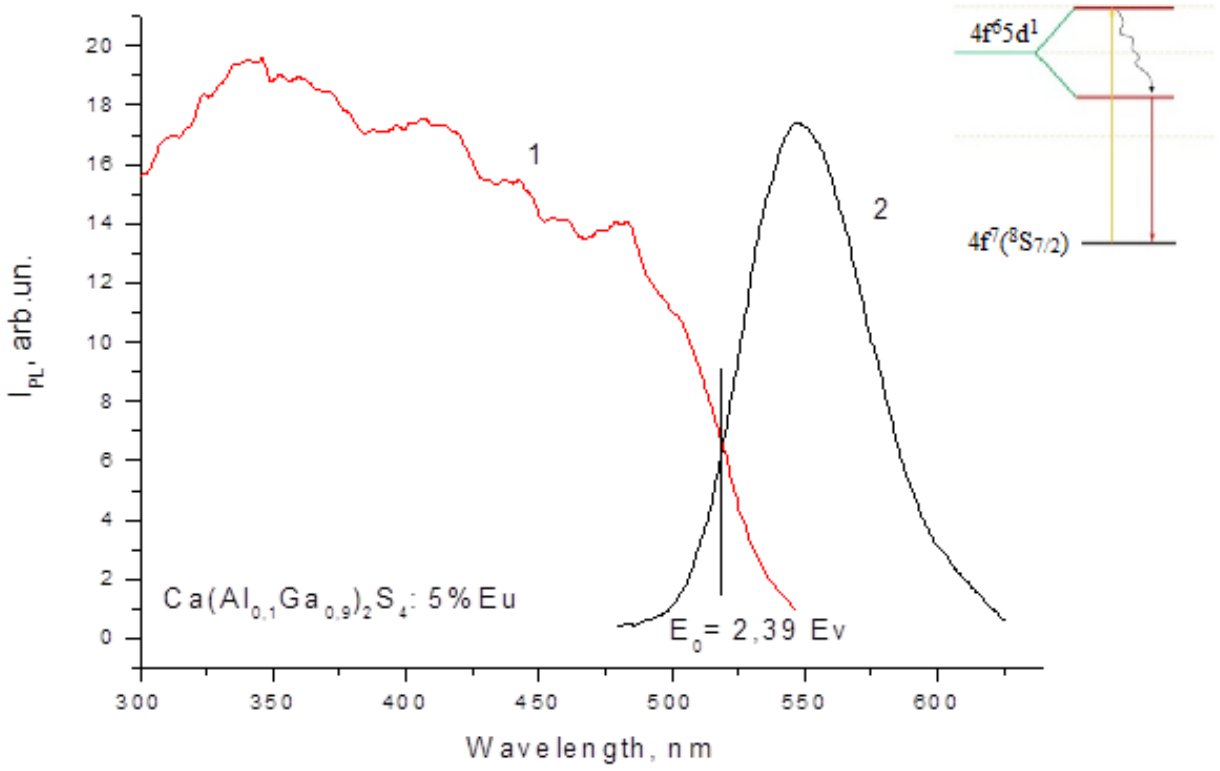

Fig.2. PhL radiation (1) and excitation spectra (2) of $Ca(Al_xGa_{1-x})_2S_4:Eu^{2+}$ (5%) crystal at T=300 K.

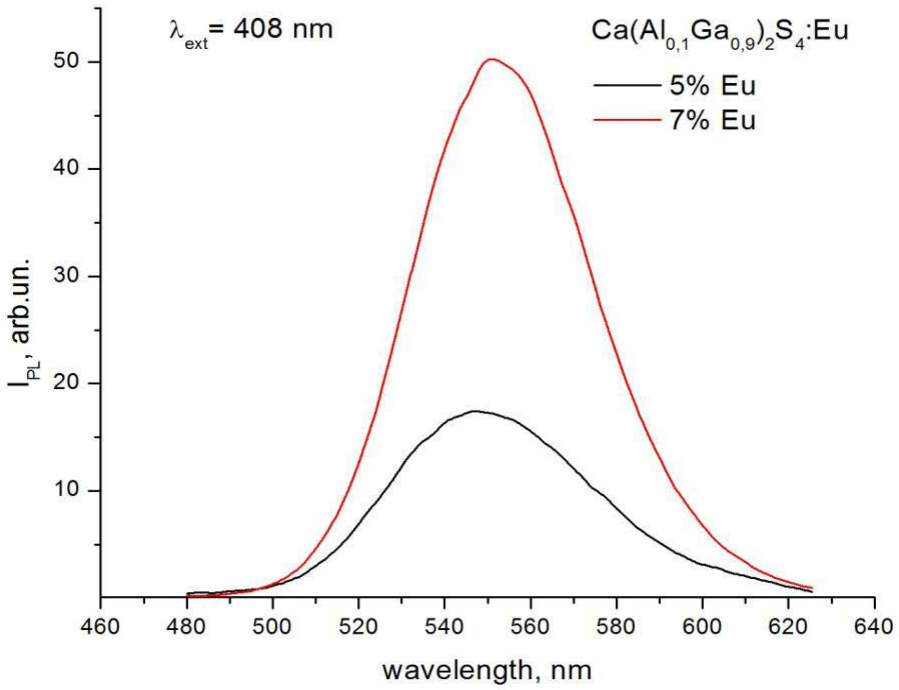

Fig.3. The photoluminescence spectra of solid solutions $Ca(Al_xGa_{1-x})_2S_4$:Eu(5%) (1), $Ca(Al_xGa_{1-x})_2S_4$:Eu(7%) (2).

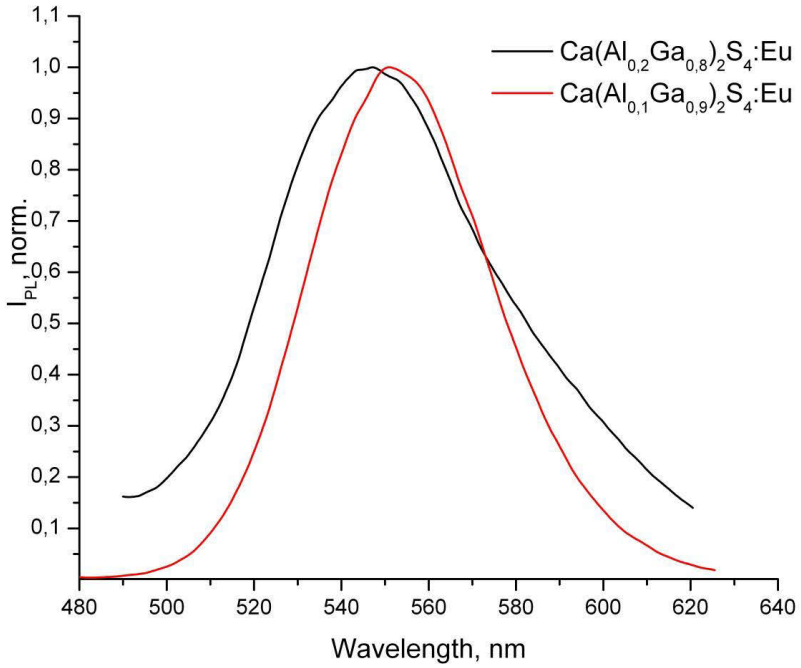

Fig.4. The dependences of photoluminescence spectra $Ca(Al_xGa_{1-x})_2S_4$:Eu on (x=Al0.1-0.2) concentration.

CONCLUSION

The energies of zero phonon line, Stokes shift and red shift are defined by investigation of PhL spectra and PhL excitation spectra, PhL band half-width on compound composition (x= 0,1 ÷ 0,2). It is established that obtained compounds have the high intensity radiation and are perspective luminophors for devices of information representation and energy-conserving light sources.

The given work is carried out at financial support of Science Development Fund under the President of the Republic of Azerbaijan - Grant№ EIF – BGM-2 –BRFTF – 1- 2012/2023 – 07/02/1Reference.

[1] *C. Ronda, T. Justel, H. Nikol.* Rare earth phosphors: fundamentals and applications. Journal of Alloys and Compounds, 1998, v. 275/277, p. 669-676

[2] *S. Saha, U. Pal, A. Chauhuri, V. Raa,* Banerjee H. Optical properties of CdTe thin films. Phys. St. Sol. (a), 1989, v.114, p.721-729

[3] *G. Zhizhin, B. Mavrin, V. Shabanov*. Optical Vibration Spectra of Crystals (in Russian), Moscow, 1984, 232 p.

[4] *X. Wu, D. Carkner, H. Hamada, I. Yoshida.* Large-screen Flat Panel Displays based on Thick-Dielectric Electroluminescent (TDEL) Technology. SID, 2004, v. XXXV, Book II, p. 1146-1149.

[5] *B.G. Tagiev, S.A. Abushov, O.B. Taqiev.* Lyumieschenchiya aktivirovannix ionami Eu^{2+}, Ce^{3+} kristallov $BaGa_2Se_4$. JPS, **77**(2010) 124 – 128. (In Russian).

[6] *R.B. Jabbarov, C. Chartier, B.G. Tagiev, O.B. Tagiev, N.N. Musayeva, C. Barthou, P. Benalloul.* Radiative properties of Eu^{2+} in $BaGa_2S_4$. Journal of Physics and Chemistry of Solids. 2005, v. **66**, Issue 6, p.1049-1056.

[7] *P. Dorenbos.* Energy of the first $4f^7 \rightarrow 4f^65d$ transition of Eu^{2+} in inorganic compounds. J. of Luminescence, 2003, v. 104, p. 239-260.

[8] *Ki-Young Ko, Young-Duk Huh and Young Rag Do.* Cathodoluminescence and Longevity Properties of Potential $Sr_{1-x}M_xGa_2S_4$:Eu (M = Ba or Ca) Green Phosphors for Field Radiation Displays Bull. Korean Chem. *Soc*. **29** (2008**)** 822 –826.

[9] *V.A. Bajenov, D.N. Karimov, R.V. Kirkin, V.N. Kolobanov, V.V. Mixaylin, S.P. Chernov.* Poverxnost, rentqenovskie sinxrotronnie i neytronnie issledovaniya. 2012, N5,s. 44 – 47. (In Russian).

Recevied: 26.05.2014

FIELD, TEMPERATURE AND FREQUENCY DEPENDENCES OF ELECTROLUMINESCENCE IN $EuGa_2S_4$

O.B. TAGIYEV[1,2], F.A. KAZIMOVA[1], T.Sh. IBRAGIMOVA[1]
[1]*Institute of Physics of Azerbaijan National Academy of Sciences*
AZ-1143, Baku, G.Javid ave., 33
[2]*M.V.Lomonosov's MSU branch in Baku*
E-mail:oktay@physics.ab.az

The investigation results of electroluminescence (EL) (field, temperature and frequency dependences of emission intensity) in $EuGa_2S_4$ crystals are presented. It is shown that EL in $EuGa_2S_4$ crystals in the dependence on electric field voltage changes as $\ln I \sim \frac{1}{\sqrt{U}}$ caused by collision ionization of Eu^{2+} ions.

Keywords: electroluminescence, rare-earth ion, electro-excitation, intensity, lifetime.
PACS: 76.30, 78.55

INTRODUCTION

The phenomenon of electroluminescence of wide-band semiconductors, in which electric field energy transforms into light, is used in different devices of semiconductor optoelectronics.

$EuGa_2S_4$ compound firstly obtained in [1] is related to wide class of substances with general formula $AB_2^{III}C_4^{VI}$(A=Eu, Yb, Sm; B=Al, Ga, In; C=S,Se,Tl). $EuGa_2S_4$ is related to tetragonal syngony (space group Fddd), the crystal lattice parameters are following: a=20,716Å, b=20,404Å and c=12,200Å[2].

The investigation results of photo-thermal-luminescence, dependence of luminescence intensity on temperature, excitation emission in $EuGa_2S_4$ crystals are given in works [3-8].

The investigation results of electroluminescence in $EuGa_2S_4$ crystals are shown in present paper.

EXPERIMENT TECHNIQUE

$EuGa_2S_4$ compound is synthesized by solid-state reaction of binary compounds EuS and Ga_2S_3. The reaction is carried out in both evacuated quartz ampoules and sublayer of activated carbon [7].

"Electroluminescent condenser" (ELC) presents itself the layered structure prepared by the following way. The luminescent layer (the mixture of luminophor and dielectric), protective (reflective) layer (the mixture of dielectric with filler) and the second non-transparent electrode are marked on glass base with current transparent layer (tin dioxide, indium oxide) being the one of electrode. The aluminum is used in the capacity of the material for the second electrode. The alternative electric voltage which luminophor excites is approached to electrodes. The emission goes out through transparent electrode and glass base.

The exciting voltage value applied to ELC depends on luminescent layer thickness, luminophor type and necessary brightness. In our case the luminophor layer by thickness 50-70 μm is obtained. For obtaining of necessary brightness the voltage 400-500V is applied in order to obtain the electric field strength by$3\cdot10^4$ V/cm order in the layer.

RESULTS AND THEIR DISCUSSION

The electroluminescence (EL) spectra of $EuGa_2S_4$ crystals are presented on fig.1. It is seen that luminescence spectrum consists on one intensive wide emission band with maximum 0,550 μm which is caused by $4f^6 5d^1 \rightarrow 4f^7$ transition of Eu^{2+} ion [7]. The energy position of this EL band coincides with energy position of photoluminescence [8].

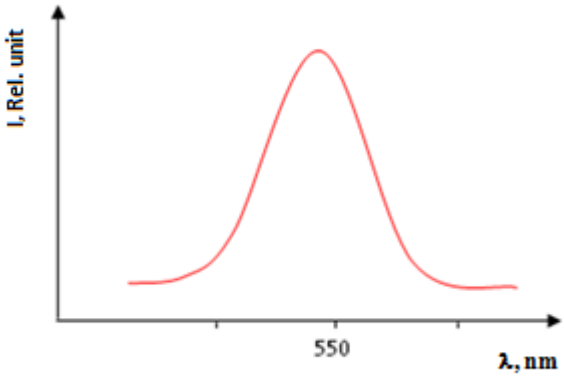

Fig.1. EL spectrum of $EuGa_2S_4$ crystal.

The dependence of emission intensity on voltage at different frequencies in $lnI \sim 1/\sqrt{U}$ coordinates is given on fig.2. The experimental points give the direct line in these coordinates, i.e. emission intensity exponentially increases with voltage and is obeyed to usual empiric formula:

$$I = I_0 \exp(-\frac{b}{\sqrt{U}}), \qquad (1)$$

where I is intensity, U is applied voltage, I_0, b are values which don't depend on voltage. The linear dependence $lnI \sim 1/\sqrt{U}$ gives us the foundation to consider that EL mechanism in our materials is caused by collision ionization of impurity centers of charge carriers accelerated by electric field. EL is observed at electric fields by $4\cdot10^4 \div 1{,}1\cdot10^5$V/cm order.

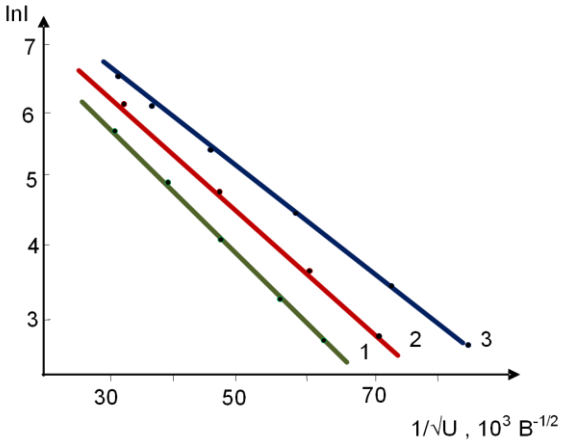

Fig. 2. Dependence of emission intensity on voltage at different frequencies in $EuGa_2S_4$ crystals: 1-200Hz, 2-300Hz, 3-400Hz

The emission intensity passes through maximum or saturates by data [9] at increase of field frequency. Some authors [10,11] reveal that emission intensity strongly changes with the exciting voltage frequency. It is supposed that such strong dependence of emission intensity on excitation frequency is connected with the emission color change. The lightening frequency characteristic is investigated at constant value of external alternative voltage.

The frequency dependence of emission intensity for $EuGa_2S_4$ compound is shown on fig.3. It is seen that in spectra the maximum is observed at frequency 3000Hz. At low frequencies the intensity increases with increase of field frequency. There are several theoretic works for interpretation of frequency dependences in narrow frequency interval [10,12].

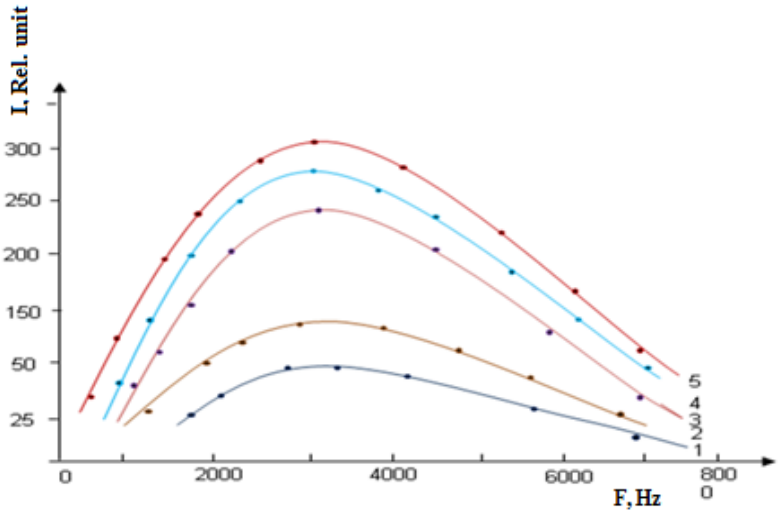

Fig. 3. Frequency dependence of emission at different voltages in $EuGa_2S_4$crystals: 1-50V, 2-400V, 3-600V, 4-800V, 5-1000V

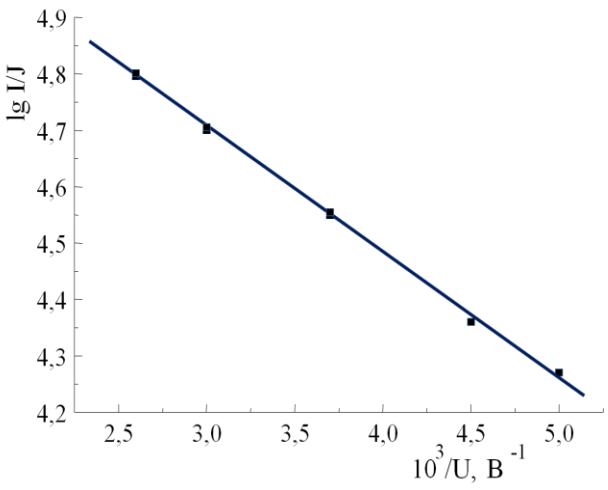

Fig.4. Dependence lg (I/J)~f(U) in $EuGa_2S_4$ crystals.

According to [12] the decrease of EL intensity at big frequencies is connected with the fact that non-equilibrium carriers injected by first voltage impulse don't have time to finish the recombination with emission centers up to appearance of second impulse and as a result of which these non-equilibrium carriers are in quasi-equilibrium state. This leads to decay of emission intensity at high frequencies

According to collision ionization theory the emission intensity is defined not only by field dependence of free carrier number but the field dependence of α collision ionization probability. In work [13] α is proportional to $exp(-nb/E^n)$ *where n* changes from 1 up to 2 and b is constant value. For such EL mechanism *lg(J/I)* value changes linearly in the dependence on U^{-n}.

Such dependence is constructed in $lg(J/I)\sim f(10^3/u)$ coordinates on fig.4. It is seen that experimental points are well marked on one direct line at $n=1$ that shows on the presence of collision ionization mechanism.

For approving of EL collision ionization mechanism the mechanism of current passing in the dependence on voltages investigated by us. That's why the experimental values of current and voltages are constructed in different coordinates. One can consider that current passing is caused by thermo-field emission mechanism so in considered structures between electrode and active material the special dielectric interlaying isn't used. There are potential barriers on the material surface causing the formation of strong electric field, which can accelerate the

charge carriers up to optical transitions. The carrying out of above mentioned regularities gives us the possibility to conclude that EL excitation mechanism is caused by inelastic collisions of hot electros with Eu^{2+} forming $EuGa_2S_4$ lattice.

The obtained experimental data are also analyzed in according with [14]. In this paper we give the formula for evaluation of trap energy depth taking part into electroluminescence studying process and their average lifetime. These parameters are defined from the dependence of emission intensity on frequency of external exciting electric voltage U:

$$I = p\exp(-\frac{q}{F}) \quad (2)$$

where $p=\frac{n_0}{\tau}\exp(-\frac{b}{\sqrt{U}})$, $q=\frac{1}{4\tau}$ is curve inclination, Fisexcitation voltage frequency. Knowing the curve inclination value $\lg I = f\left(-\frac{1}{F}\right)$ one can evaluate average trap lifetime.

$$\tau = \frac{1}{4q} \quad (3)$$

The trap lifetime is expressed through activation energy by following way [13]:

$$\tau = \frac{1}{S}\exp(\frac{E}{kT}) \quad (4)$$

where S is frequency factor, κ is Boltzmann coefficient, E is activation energy, T is temperature. Using the expression (3) and (4) for E we obtain:

$$E=2,3\kappa T\, lg(\frac{S}{4q}) \quad (5)$$

In these formulas the important trap parameters are defined (activation energy is 0,8eV, τ=50мкс).

CONCLUSION

The carrying out of above mentioned regularities gives us the possibility to conclude that EL excitation mechanism is caused by inelastic collisions of hot electrons with Eu^{2+} forming $EuGa_2S_4$ lattice.

The given work has been supported by Science Development Foundation under the President of the Republic of Azerbaijan Grant № EİF-BGM-2- BRFTF-1-2012/2013-07/02/1.

[1] *R. Eholie, O. Gorochov, M. Guittard, A. Mazuzier, J. Flahaut.* Les composesde type $PbGa_2Se_4$; EuM_2X_4; Sr M_2X_4 et PbM_2X_4 (avec M=Al, Ga et X=S,Se). Bull. Cos. Chim. Fr.1971, №3, P.747-1750.

[2] *R. Roques, R. Rimet, J.P. Declercq et G. Germain.* Determination de la structure crystalline de $EuGa_2S_4$. Acta. Cryst., 1979. B.35, p.555-557.

[3] *Q.B. Abdullaev, O.B. Tagiev, Q.M. Niftiev, O.M. Aliev.* Fotolyumineschenchiya monokristallov $EuGa_2S_4$. JPS, 1985, 53, v.1, s.157. (in Russian).

[4] *O.B. Tagiev, G.M. Niftiev, I.M. Askerov*. The Frenkel thermal–field emission $EuGa_2S_4$. Phys.stat.sol.(a), 1983,78, №1, k43-k46.

[5] *O.B. Tagiev, G.N. Ibragimova.* Optical properties of $EuGa_2S_4$. Phys.Stat.sol.(a), 1986,97, №1, k 49-k 52.

[6] *A.N. Qeorbiani, B.Q. Taqiev, O.B. Taqiev, S.A. Abushov, F.A. Kyazimova, T.Sh. Qashimova, S.Syuyun (Xu Xurong).* Neor.mat. 2009, t.45, №2, s.152-158.

[7] *C. Barthou, P. Benalloul, B.G. Tagiev, O.B. Tagiev, et.al.* Energy transfers betveen Eu^{2+} and Er^{3+} in $EuGa_2S_4$: Er. J. of Physics: Condensed matter. 2004, 16, p.8075-8084.

[8] *A.N. Qeorobiani, S.A. Abushov, F.A. Kazzimova, B.Q. Taqiev, O.B. Taqiev, P. Benaloul, K. Bartou.* Lyumineschenchiya $Ga_2S_4:Er^{3+}$. Neorq.mat. 2006, t.42, №11, s. 1304-1307. (In Russian).

[9] Sol.Nudelman Frank Matossi. Time-Average Electroluminescence out put of some zinc sulfide phosphor. J.Electrochem.Soc., 1956, 103, №1, p.34-38.

[10] *A.Q. Qoldman.* Noviy effekt elektrolyumineschenchii chernoqo karborunda. DANSSSR. 1960, 135, №5, s.1108-1110. (In Russian).

[11] *J.F. Waymonth.* Optical measurementso on electroluminescent zinc sulfide. J. Electrochem.Soc., 1953, 100, №2, p.81-84.

[12] *G.G. Harman, R.L. Ragbold.* Measurement of Minority Carrier lifetime in SiC by a novel electroluminescent method. // J.appl. Phys., 1961, 32, №6, p.216-217.

[13] *N.A, Vlasenko Z.L. Denisova, V.S. Khomchenko.* Electroluminescence of SiO_x-LnF_3 Thin film. Phys.stat. sol (a), 1984, 81, №2, p.657-660.

[14] *R.P. Khare and M. Khare.* A new method of analysis of traps taking part in the electroluminescence process. J.Phys. stat. sol.(a) 1981, v.65, p.725-729.

Received: 01.05.2014

MAGNETO-OPTICAL PROPERTIES OF SINGLE CRYSTALS $Cd_xHg_{1-x}Te$ ($0{,}18 \le x \le 0{,}30$)

G.S. SEYIDLI, N.M. SHUKUROV*, M.Sh. GASANOVA*

Azerbaijan Teacher Institute

**Azerbaijan Technical University*

E-mail:geneticsster@gmail.com.mhsh28@mail.ru

The article is dedicated to experimental investigation of Faraday rotation in range of wavelength $6 \div 14$ μm on $Cd_xHg_{1-x}Te$ $(0{,}18 \le x \le 0{,}30)$ samples at 300K. It is established that experimental dependences x on sample thickness d in single crystals $Cd_xHg_{1-x}Te$ with $(0{,}18 \le x \le 0{,}30)$ at $T = 300K$ the nonmonotonous change of x with decrease of sample thickness. This is experimentally approved by the presence of large-scale, nonhomogeneous regions by their composition inside crystals.

Keywords: Faraday effect, intrinsic conductivity, composition fluctuation, charge carrier concentration, angle of rotation of polarization plane, Verdet constant

PACS: 61.72.V; 72.80.E

The successes of modern science and technique are connected with application of different solid-state infrared detector for formation of which the semiconductors with narrow forbidden band are the most perspective ones. Among these materials it is necessary to emphasize the solid solutions $Cd_xHg_{1-x}Te$ in which one can gradually regulate the forbidden band width in wide interval (from -0,30 up to + 1,60 eV) by the way of component content change. Nowadays according to requirements of special technique to formation of high-sensitive infrared detector, the practical application of $Cd_xHg_{1-x}Te$ is strongly overrun the comprehensive study its physical properties. That's why the experimental investigation of magneto-optical properties of $Cd_xHg_{1-x}Te$ single crystals and also the formation of new photodetectors on their base is the actual one from both scientific and practical point of view. It is known that Faraday effect on free charge carriers is used for finding of charge carrier effective mass value, its concentration and temperature dependence [1].

The physical substance of Faraday effect is in the rotation of polarization plane of linearly polarized radiation at its propagation through substances being in magnetic field parallel to radiation propagation direction. Moreover, the angle of rotation of polarization plane one can expressed by Verdet constant which enters into empirical law: $\varphi = \theta \cdot H \cdot d$, where H is magnetic field strength, d is sample thickness.

Thus, the definition of Faraday effect value leads to measurement of three values: angle of rotation of polarization plane, magnetic field strength and crystal thickness. The measurement of two last values is well-known and carried out independently. For Faraday effect investigation for our samples the experimental installation constructed on the base of monochromator SPM-2 of Zeiss firm and having the series of prisms that allows us to measure in wavelength region from 0,2 up to 50μm is used [1].

To investigate of Faraday rotation caused by free charge carriers in solid solutions $Cd_xHg_{1-x}Te$ under influence of strong electric field, the functional abilities of measuring installation are widened by the way of application of electromagnet between gaps of which the nitrogen cryostat with investigated sample is put. The magnet field is varied from 0 up to 1,0Tl.

The electric filed applied to the samples changes from 0 up to $5 \cdot 10^2 B/cm$. The polarizers of IR-radiation $MLP-1$ having the polarization coefficient in 95% order are applied as polarizer and analyzer. The gas laser working in continuous mode with wavelength 10,6 μm is used in the capacity of IR-radiation.

The polarizer and analyzer are situated under the angle $\alpha = 45^0$ to each other in given one-beam scheme of φ angle definition. In this case the intensity change $dJ/d\alpha$, which is described by Malus equation, $dJ(\alpha)/d\alpha = J_{11} \cdot \cos^2 \alpha$ is maximum one and relative intensity change is defined by following expression $\Delta J / J = 2tg\alpha \ \Delta\alpha$.

In the given experiment the definition technique of angle of rotation of polarization plane is as follows: the polarizer plane of polarization is situated under angle α to analyzer plane.

The light flux of intensity $J_0 = J_{11} \cdot \cos^2 \alpha$ goes into photodetector. Further, the magnetic field in direct and reversal direction is switched on.

Moreover, the intensity variation of former radiation analyzer on $\delta J = \Delta J \uparrow -\Delta J \downarrow$ value takes place, which is written on recorder for measurement precision. The angle α is obtained from the calculation of intensity variation for two directions of magnetic field:

$$\Delta J = J_{11} \cdot \cos^2(\alpha \pm \varphi) - J_{11} \cdot \cos^2 \alpha \qquad (1)$$

The signal total relative change at two directions of magnetic field is defined by the following expression:

$$\frac{\Delta J}{J_0} = \frac{J_{11}\left\{\left[\cos^2(\alpha+\varphi) - \cos^2\alpha\right] - \left[\cos^2(\alpha-\varphi) - \cos^2\alpha\right]\right\}}{J_{11} \cdot \cos^2\alpha} = 2tg\alpha \cdot Sin2\varphi. \qquad (2)$$

At small angles of rotations $(\varphi \le 10^0)$ and $\alpha = 45^0$, from expression (2) we have:

$$\alpha = \frac{\Delta J}{4J_0} \cdot \frac{pad}{cm} = \frac{45^0}{\pi} \cdot \frac{\Delta J}{J_0} \cdot \frac{qrad}{cm} \qquad (3)$$

Thus, in order to measure the rotation on 1^0 it is necessary to fix the relative intensity change in 1/14,33 times. It is necessary to note that obtained expression (3) is related to ideal polarizer case. The polarization degree of polarizer is taken into consideration in real polarizers $P = \frac{J_{11} - J_\perp}{J_{11} + J_\perp}$. This is connected with the fact that photodetector registers the intensity the both polarized and non-polarized radiation parts whereas angle of rotation of polarization plane is defined by only radiated polarized component. The taking into consideration the polarization is reduced the formula (2) into the following form:

$$\frac{\Delta J}{J_0} = 2pSin2\varphi, \quad \text{for angles}$$

$$\varphi \le 10^0, \varphi = \frac{4J}{4PJ_0} \qquad (4)$$

Thus, the measurement error of angle of rotation is defined mainly by error in definition of intensity flow change ΔJ and the flow itself value J_0. In our case the experiment error doesn't exceed 10%.

The measurements of Faraday rotation are carried out at room temperatures in wavelength range 6-14μm on samples $Cd_xHg_{1-x}Te$ of n- and p –type of conduction $(0,18 \le x \le 0,30)$, grown up by the method of slow cooling at constant temperature gradient along ingot. The sample thickness is 100-200μm.

The polarization angle in magnetic field one can calculate from expression [1].

$$\theta_3 = \frac{\varphi}{H \cdot d} = -\frac{2\pi e^3 \cdot N}{c^2 \cdot n \cdot \omega} \cdot \frac{H}{(m^*)^2} \qquad (5)$$

where ω is electromagnetic wave frequency; n is refraction coefficient; C is light velocity; e is electron charge; H is magnetic field strength; θ_3 is Verdet constant; d is sample thickness.

The spectral dependence of Faraday rotation in semiconductors is defined by three components [1]:

$$\theta = \theta_1 + \theta_2 + \theta_3 \qquad (6)$$

where θ_1 is interband Faraday rotation:

$\theta \infty \left[E_g^2 - (\hbar\omega)^2\right]^{-1}$: Eg is forbidden band width; θ_2 is Faraday rotation value not depending on radiation length; θ_3 is defined by expression (5). For $Cd_xHg_{1-x}Te$ crystals at $\omega \to \infty$ the value $\theta_3 \to 0$.

That's why at Faraday effect investigation in dependence on light wavelength under $\hbar\omega < E_g$ condition one can define m^* from [2] at known N and n. The spectral dependences $\varphi(Hd)$ on λ^2 for samples of thickness 100μm (fig.1) show that section sizes are defined by both the composition of single crystals $Cd_xHg_{1-x}Te$ (points of intersection shift to the side of short-length waves at x increase) and charge carrier concentration in them with decrease of short-length waves at intersection of curves with abscissa axis.

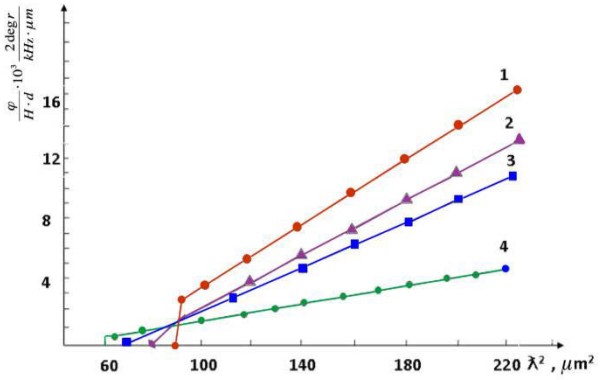

Fig 1. The dependences of angle of Faraday rotation on light wavelength in crystals $Cd_xHg_{1-x}Te$ at $T = 300K$ x,1 – 0,18 : 2 – 0,20 : 3 – 0,24 : 4 – 0,28.

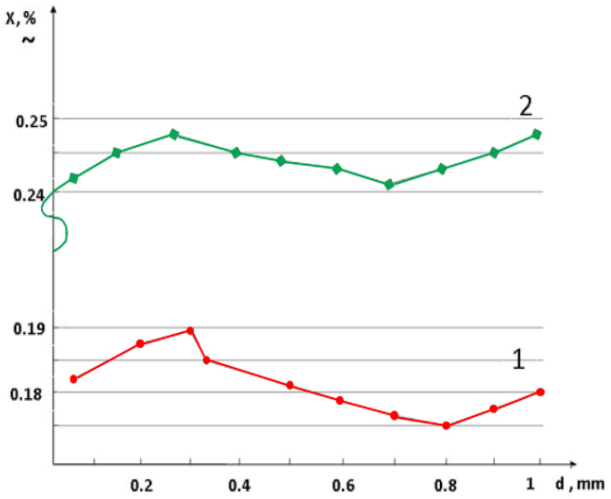

Fig.2. The dependence of $Cd_xHg_{1-x}Te$ composition on sample thickness. x : 1 – 0,18 : 2 – 0,27 : T = 80K

This is caused by influence of interband Faraday effect (θ_1) [3]. Values m^* defined in long-wave spectrum region are $x = 0,18,\ 0,20,\ 0,24, 0,28$ $m^* = 0,016m_0,\ 0,017m_0,\ 0,020m_0,\ 0,028m_0$ correspondingly.

The investigation of Faraday effect on free charge carriers gives the possibility to define x and its fluctuation Δx in single crystals $Cd_xHg_{1-x}Te$ because in temperature regions where the samples have their intrinsic conductivity, the concentration of eigen carriers causing Faraday effect are defined by forbidden band width and correspondingly by x value in these crystals: i.e. Eg, N and θ values are function on x.

The measurement of $x \approx f(d)$ dependence allows us to establish the fluctuation amplitudes in relative units in different crystals $Cd_xHg_{1-x}Te$ From experimental dependences $x \approx f(d)$ in single crystals $Cd_xHg_{1-x}Te$ with $x = 0{,}18$ and $0{,}24$ at $T = 80K$ (fig.2) it is seen the nonmonotonous variation x with decrease of sample thickness, i.e. the presence of large-scale nonhomogeneous regions by components inside crystals is proved.

The composition fluctuation amplitude in these crystals decreases with increase of CdTe content in solid solution. The given experimental results show that crystal composition and its fluctuation by sample thickness can be evaluated with the help of Faraday effect on free charge carriers.

[1] *F.F. Sizov, Yu.N. Uxananov.* «Maqnitoopticheskie effekti Fradeya i Foqta v primenenii k poluprovodnikam» Kiev, Nauk. dumka, 1979, 179 s. (in Russian).

[2] *W. Shockley,* Belle Syst.Journ.,28,435(1949).

[3] *Yu.N. Uxananov*. Opticheskie svoystva poluprovodnikov; Iz-vo Nauka, 1977, 366 s. (in Russian).

Recevied: 05.05.2014

OPTICAL PROPERTIES OF CHALCOGENIDE GLASSY SEMICONDUCTOR $Se_{95}Te_5$ DOPED BY SAMARIUM

A.I. ISAYEV, S.U. ATAYEVA*, S.I. MEHDIYEVA, V.Z. ZEYNALOV
Institute of Physics of Azerbaijan National Academy of Sciences
AZ-1143, Baku, G.Javid ave., 33
e-mail: seva_atayeva@mail.ru

The optical width of "forbidden band", refraction index and extinction index are defined by investigation of optical transmission spectrum of chalcogenide glassy semiconductor (CGS) $Se_{95}Te_5$ doped by samarium. E_0 is oscillator energy connected with energy gap and E_d is dispersion energy characterizing the interband transition force, are defined within the framework of one-oscillator model. The influence of samarium impurity on optical and dispersion parameters can be connected with peculiarity of impurity atom distribution, changes of chemical band and coordination number.

Keywords: forbidden band width, extinction coefficient, dispersion parameters
PACS: 68.37.Ps 68.55.-a 78.20.-e

INTRODUCTION

Nowadays the amorphous and glassy selenium as typical representative CGS materials is intensively investigated [1-3]. However, the obtained results don't agree with each other that prevent its many-functional usage in practical aims. This is, first of all, connected with its various structural elements, i.e. with the existence of ring and chain molecules of different dimension and also big concentration defects with negative correlation energy (U^-- centers) appearing as a result of the presence of dangling bonds. The relative composition of structural elements depends on technological process regime of sample preparation and presence of controlled and non-controlled impurities. The additions of iso-electronic (sulfur and tellurium) and branching (arsenic) elements [4-5] and impurities revealing in the ion forms (halogens and rare-earth elements) [6-8] lead to changes in local structure (dimensions and macromolecule numbers) and U^-- concentrations of centers. All above mentioned allow us to change directly the electron properties of given semiconductor and increase its crystallization stability that it is necessary for enlargement of range of application.

The present paper is dedicated to investigation of CGS optical properties of $Se_{95}Te_5$ material doped by samarium. The choice of given CGS in the capacity of investigation object is caused by this circumstance that tellurium addition significantly changes the optical and photoelectrical properties of amorphous selenium [5,9]. In particular, the optical forbidden band width and refractive index change and also the photo-sensitivity strongly increases. The samarium usage for doping is connected with the fact that samarium as chemically active element and revealing the two and three valences it should form the new structural elements with selenium and tellurium atoms. Thus, the addition of tellurium and doping element samarium should lead to structure modification of amorphous selenium that allows us to find the methods of electron property control.

CGS optical properties of $Se_{95}Te_5$ composition doped by samarium are investigated in present paper, in particular, the "forbidden band" optical width, refractive index, extinction index are defined. The dispersion parameters, which connect with atom, electron material structure and energy spectrum of electron states, are defined also. The knowledge of given parameters also plays the important role in checking of material perspective in optoelectronics.

EXPERIMENT TECHNIQUE AND SAMPLE PREPARATION

CGS synthesis of $Se_{95}Te_5$ composition doped by samarium (0,05; 0,1; 0,25; 0,5; 1 at%) is carried out in the following sequence: essentially pure elementary substances in corresponding atomic percentage are filled in quartz ampoules and after air evacuation up to pressure 10^{-4} millimeter of mercury during three hours are heated up to temperature 900-950 ^{0}C with following 12-hour soaking. The synthesis is carried out in rotary furnace and cooling is carried out in regime of switched off one with the aim of sample homogeneity supply. The films by thickness 3mm used in the investigation are obtained by thermal evaporation with velocity 0,3 – 0,4 μm /min. The optical transmission spectra are investigated by double-beam spectroscopy method in energy interval 1 ÷ 2,8 eV. All experiments are carried out at room temperature.

RESULTS AND THEIR DISCUSSION

CGS transmission spectra of $Se_{95}Te_5$, $Se_{95}Te_5Sm_{0,1}$, $Se_{95}Te_5Sm_{0,25}$, $Se_{95}Te_5Sm_1$ compositions (in $Se_{95}Te_5$ samples containing the other concentrations of samarium atoms the similar interferential pictures are observed)are shown in fig.1.

As it is seen from the picture beginning from value of incident light wavelength 700nm the interferential maximums and minimums are observed in spectra that allows us to calculate such optical coefficients as refractive index and extinction index by method supposed in work [10].

According to [10] the refractive index in spectrum region of corresponding photon energy where light is weakly absorbed is expressed by formula:

$$n = [N + (N^2 - S^2)^{1/2}]^{1/2}, \quad (1)$$

where

$$N = 2S(T_M - T_m)/(T_M T_m) + ½(S^2 + 1) \qquad (2)$$

T_M and T_m are transmission coefficients corresponding to interferential maximums and minimums correspondingly in transmission spectrum:
The extinction index k is obtained by formula:

$$k = \frac{\alpha\lambda}{4\pi} \quad . \qquad (3)$$

For definition of the dependence of refractive index on wavelength in short-wave region, the empiric formula given in work [10-11] is used:

$$n = a + b/\lambda^2 \quad , \qquad (4)$$

where λ is wave length in vacuum; a, b are constants, the values of which for each material should be defined from the experiment. The graph of refractive index dependence on wavelength corresponding to (4) equation is shown on fig.2a. As it is seen from the figure the refractive index value decreases with wavelength increase, i.e. the normal dispersion is observed.

According to [12-13] the dispersion of optical parameters within framework of one-oscillator model is well described by the following expression:

$$\boldsymbol{n^2} = 1 + \frac{\boldsymbol{E_0 E_d}}{\boldsymbol{E_0^2 - E^2}} \quad , \qquad (5)$$

where E is photon energy, E_0, E_d are parameters of one-oscillator model. In this expression, E_0 denotes oscillator energy connected with average energy gap, i.e. with chemical bond energy between atoms in amorphous matrix. E_d is dispersion energy characterizing the interband transition force. It is necessary that formula (5) is successfully used for interpretation of dispersion parameters of both crystalline and amorphous materials [12-13]. The dependence graphs $(n^2 - 1)^{-1}$ on E^2 ,where $(E_0.E_d)^{-1}$ is defined on curve inclination and E_0/E_d is defined on the crossing with ordinate axis (fig. 26) are used for finding of dispersion parameters.

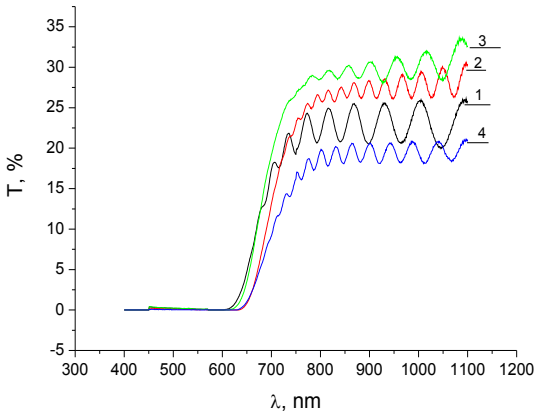

Fig.1. Transmission spectra of $Se_{95}Te_5$ with impurity different composition of Sm: *1*- $Se_{95}Te_5$, 2-$Se_{95}Te_5Sm_{0.1}$, *3*-$Se_{95}Te_5Sm_{0.25}$, *4*- $Se_{95}Te_5Sm_1$, at room temperature.

Firstly it is shown by author of work [15] that in CGS As_x Se_{100-x} system between oscillator energy and optical forbidden band width defined by Tauz method [14] the relation $E_0 \approx 2E_g$ takes place.

Further it is revealed that given relation takes place for other chalcogenide glassy films [16-17]. Our investigations show that the given relation is also right for $Se_{95}Te_5$ composition doped by samarium.

According [12-13] E_d depends on imaginary part of dielectric constant that one cannot say about E_0, i.e. the interconnection between E_d and E_0 is absent.

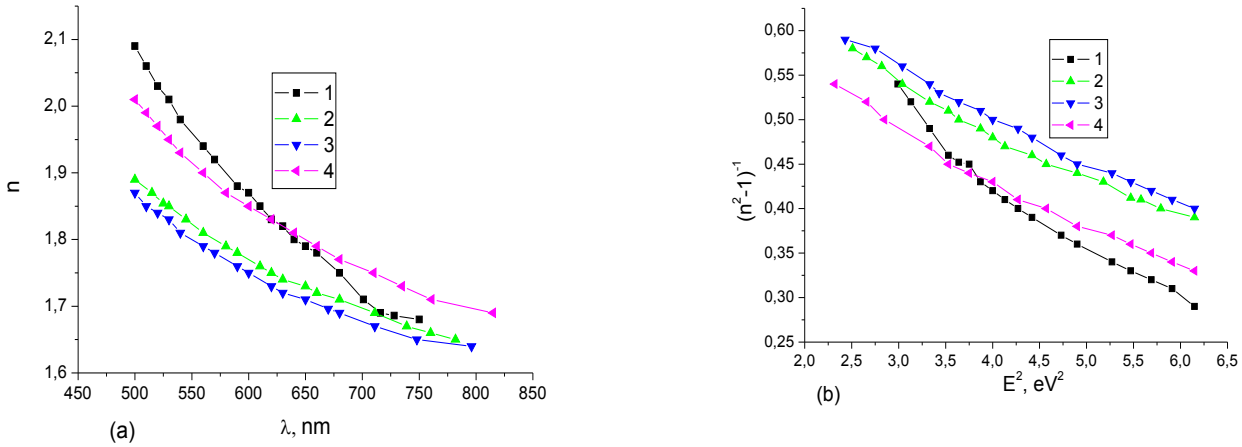

Fig.2. Spectral dependences of refractive index (a) and dependences $(n^2-1)^{-1}$ on E^2 (б) of CGS with impurity different composition of Sm: *1*- $Se_{95}Te_5$, 2- $Se_{95}Te_5Sm_{0.1}$, *3*- $Se_{95}Te_5Sm_{0.25}$, *4*- $Se_{95}Te_5Sm_1$.

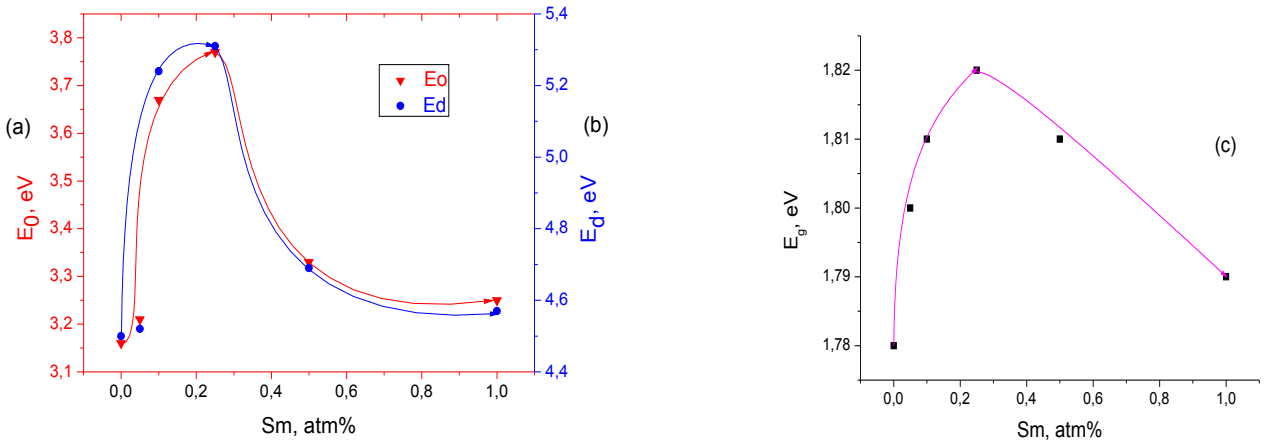

Fig.3. Dependences of dispersion parameters E_0 (a), E_d (b) and optical width of forbidden band E_g (c) on Sm atom concentration.

.

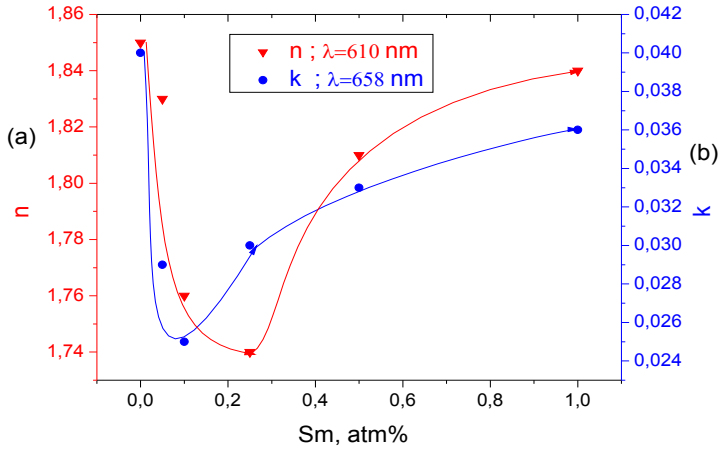

Puc. 4. Dependences of optical parameters: refractive index n (a) and extinction index k (b) for $Se_{95}Te_5Sm_x$ on composition.

The dependences of dispersion parameters E_0 (fig.3a), E_d (fig.3b) and E_g (fig3c) on samarium atom concentration are presented on fig.3. The dependences of refractive index (n) (fig.4a) and extinction index (k) (fig.4b) on samarium atom concentration are shown on fig.4. As it is seen from the figures 3-5, all curves have extremums, i.e. the influence of atom impurities on the given parameters has the complex character. E_0, E_d and E_g increase with increase of samarium atom concentration and n and k decrease. The further increase of samarium atom concentration lead to decrease of E_0, E_d and E_g increase of n and k.

For explanation of obtained results the cavitated-cluster Eliot model and also Penn model are applied. According to cavitated –cluster Eliot model [18-20] there are ~~–e~~avities" the dimensions of which are less than one nanometer in CGS materials [19,22]. Such structure allows us to attract Penn model [23] supposed for materials containing pores with dimensions less than nanometer. According to Penn theory the statistic refractive index is expressed in the following form:

$$n_0^2 = 1 + {}^2/_3 \left(\frac{\omega_p}{\omega_g}\right)^2 \quad . \qquad (6)$$

where ω_p is plasma frequency, $h\omega_p$ is Plasmon energy characterizing the collective excitation of electron gas localized of nanometer dimension heterogeneities where the definite order in atom disposition takes place (average order). The density of the given regions is bigger than average density of the given material. That's $h\omega_p$ can serve as a measure of microscopic density of amorphous materials and $h\omega_g$ is Penn energy band. Plasma frequency is expressed by the following formula:

$$\omega_p = \frac{4\pi e^2 \rho}{m\ A} N_A\ n_v \quad , \qquad (7)$$

where n_v is number of valence electrons per atom; N_A is Avogadro number, e is electron charge, m is electron mass, ρ is material density, A is molecular mass.

According to [13] for materials with pores of diameter

0,5nm which is character for CGS materials [22] the plasma frequency is expressed in the form:

$$n = 1 + 2/3\left(\frac{\omega_p^2}{\omega_g^2}\right)\left(\frac{\rho}{\rho^0}\right)^{1-4f} \quad , \qquad (8)$$

where $f = dlnC / dln\ \rho$ is cluster bond part per pore surface, C is coordination number, index "zero" denotes the parameter of totally coordinated substance. f value changes from 0 up to 1 in the dependence on cavity dimensions. For our samples $f = 0{,}25$. According to last equation, n of such material is more than of material of totally coordinated substance. Such fact one can see if we pay attention on fig.2 where at increase of samarium concentration in CGS composition $Se_{95}Te_5$ n and k firstly decrease (up to 0,25%) and increase in the following stage. Amorphous $Se_{95}Te_5$ as a representative of CGS materials has the dangling bonds, which is explained by charged centers with negative correlation energy (U^- are centers) and also cavities of diameter less one nanometer. Samarium atoms in small concentrations mainly fulfill the existing cavities and stitch the chain molecules because of chemical activity. Thus, the density deficiency is eliminated and also part of chemical bonds of Se-Te and Se- Se with small energy exchange by Sm-Te, Sm-Se bonds with big energy that leads to E_0 increase. Chemically active element samarium atoms stitch the chain molecules consisting of atoms of selenium and tellurium. The average coordination number increases that leads to E_d increase and n and k decrease. The big concentrations of samarium atoms chaotically spreading along whole matrix in the form of positively charged ions increase the concentrations of U-centers, as a result of which the local state concentrations in energy gap increases and the fluctuation of electrostatic potential intensifies. This leads to decrease of E_0, E_d and E_g and increase of n and k.

CONCLUSION

The refraction index and extinction index are obtained by investigation of transmission spectra CGS of $Se_{95}Te_5$ composition doped by samarium (0,05; 0,1; 0,25: 0,5; 1at%). E_0 is oscillator energy connected with average energy gap and E_d is dispersion energy characterizing the interband force are defined within framework of one-oscillator model. Structural peculiarities ChGS, i.e. the existence of cavities by diameter less than nanometer (Eliot model) in samples allows to us to interpreter the concentration dependence of optical parameters (n, k, E_g) and dispersion parameters in limits of Penn model. It is concerned that samarium atoms in small concentrations mainly fulfill the cavities and stitch the chain molecules because of chemical activity, the part of chemical bonds Se-Te and Se- Se with less energy are exchanged by bonds with bigger energy Sm- Te, Sm-Se. This causes to elimination of density deficiency and increase of coordination number that is accompanied by n and k decrease and increase of E_0, E_d and E_g. The big concentrations of samarium atoms chaotically spreading along whole matrix in the form of positive charged ions increase concentrations of U^-centers. As a result of this fact the concentration of local states in energy gap increases and the fluctuation of electrostatic potential increases that leads to E_0, E_d and E_g decrease and increase of n,k.

[1] *J. Hegedus, K. Kohary, D. G. Pettifor, K. Shimakawa, S. Kugler.* Photoinduced Volume Changes in Amorphous Selenium// Phys. Rev. Lett.V 95, 206803- Published 8 November (2005).

[2] *J. Hegedus, K. Kohary, S. Kugler.* Universal feature of photo-induced volume changes in chalcogenide glasses// J. Non- Cryst. Solids. V.352, P.1587-1590(2006).

[3] *R. Lukacs, M. Veres, K. Shimakawa, and S. Kugler.* Photoinduced bond breaking in a-Se: Raman spectroscopic study// Phys. Status Solidi C 8, N9, P.2789-2791(2011).

[4] *K.D. Chendin.* Elektronnie yavleniya v xalkoqenidnix stekloobraznix poluprovodnikax. // Otv. Red., Sankt-Peterburq, s. 320, Nauka (1996). (In Russian).

[5] *Q.B. Abdullaev, D.Sh. Abdinov.* Fizika selena. «Elm» Baku-1975. (In Russian).

[6] *L.P. Kazakova, E.A. Lebedov, A.I. Isaev, S.I. Mextieva, N.B. Zaxarova, I.I.. Yatlinko.* Vliyanie primesey qaloqenov na perenos nositeley zaryada v stekloobraznix poluprovodnikax sistemi *Se-As*// FTP T.27, vipusk 06, s.959 (1993). (In Russian).

[7] *L.P. Kazakova, E.A. Lebedev, N.B. Zakharova, I.I. Yatlinko, A.I. Isayev, S.I. Mekhtiyeva.* Improvement of charge transport in Se-As glasses by doping with halogens// J. of Non – Cristalline solids V.167, P.65-69 (1994).

[8] *A.I. Isayev, S.I. Mekhtieva, N.Z.Jalilov, R.I. Alekperov, G.K. Akberov.* Localised states in the band gap ot chalcogenide glass-like semiconductors of Se-As system with Sm impurity// Solid State Communications V.149, ISS 1-2, P.45-48 (2009).

[9] *A. Mendoza-Galvan, E. Garcia-Garcia, Y. V. Vorobiev, J. Gonzalez-Hernandez. Structural*, optical and electrical characterization of amorphous Se_xTe_{1-x} thin film alloys// Microelectronic Engineering V.51-52, P.677-687 (2000).

[10] *R. Swanpoel.* Determination of the thickness and optical constants of amorphous silicon// J. Phys. E: Sci. Instrum, V.16, N12, P.1214 (1983).

[11] *R. Swanpoel.* Determination of surface roughness and optical constants of inhomogeneous amorphous silicon films// J. Phys. E: Sci. Instrum, V.17, N10, P.896 (1984).

[12] *S.H. Wemple and M. DiDomenico.* Behavior of the Electronic Dielectric Constant in Covalent and lonic materials// Phys. Rev. B 3, P.1338 (1971).

[13] *S.H. Wemple.* Refractive- index Behavior of amorphous Semiconductors and glasses// Phys. Rev. B7, P.3767 (1973).

[14] *D.L. Wood and J. Tauc.* Weak absorption tails in

amorphous semiconductors// Phys. Rev. B5, P.3144-3151 (1972).

[15] *K. Tanaka*. Optical properties and photoinduced changes in amorphous As-S films// Thin Solid Films, V.66, Iss.3, P.271-279 (1980).

[16] *J.M. Gonzalez-Leal, A. Ledesma, A.M. Bernal-Oliva, R. Prieto-Alcon, E. Marquez, J.A. Angel, and J. Carabe*. Optical properties of thin- film ternary $Ge_{10}As_{15}Se_{75}$ chalcogenide glasses// Mater. Lett. V.39, P.232-239 (1999).

[17] *T.I. Kosa, T. Wagner, P.I.S. Ewuen and A.E. Owen*. Index of refraction of Ag- doped $As_{33}S_{67}$ films: Measurement and anaiysis of dispersion// Philos. Mag. V.71, Iss.3, P.311-318 (1995).

[18] *S.R. Elliott.* Medium- range structural order in covalent amorphous solids// Nature V.354, P.445-452 (1991).

[19] *S.R. Elliott.* Extended- ranqe order, interstitial voids and the first sharp diffraction peak of network glasses// J. Non-Cryst. Solids. V.182, P.40-48 (1995).

[20] *E.A. Smorqonskaya, K.D. Chendin.* Elektronnie yavleniya v xalkoqenidnix steklloobraznix poluprovodnikax// Otv. Red. Chendin K.D., RAN**,** SPb:Nauka, S. 9, 486 (1996). (In Russian).

[21] *S.R. Elliott.* The origin of the first sharp diffraction peak in the structure factor of covalent glasses and liquids// J. Phys. Cond. Mat., V.4,N 38, P.7661 (1992)

[22] *A.R. Alekberov, A.I. Isaev, S.I. Mextieva, Q.A. Isaeva, Q.Q. Quseynov, A.S. Amirov.* AMEA Xeberler, XXXIII, №2, S.44-56 (2013). (In Russian).

[23] Fizika qidroqenizirovannoqo amorfnoqo kremniya. Vip. 2: Elektornnie I kolebatelnie svoystva. Pod red. Dj. Djounopulosa, Dj. Lyukovski – M.; Mir, s. 447 (1988). (In Russian).

[24] *J.C. Philips.* Electronic Structure and Optical Spectra of Amorphous Semiconductors // Phys. St. Sol. (b), Vol.44, P.K1–K (1971).

Recevied: 02.05.2014

PHOTOLUMINESCENCE OF SOLID SOLUTIONS $Ca_{0.5}Ba_{0.5}Ga_2S_4$: Eu,Er

G.P. YABLONSKI[1], M.S. LEONENA[1]
Institute of Physicsnamed after B.I.Stepanova of Belarus NAS
Independence ave.,68,220072, Minsk, Belarus
B.G. TAGIYEV[2], O.B. TAGIYEV[2,3], T.G. NAGIYEV[2], S.G. ASADULLAYEVA[2]
Institute of Physics of Azerbaijan NAS AZ1143,
G.Javid ave.,33,Baku, Azerbaijan
e-mail:tural@nagiyev.net
M.V. Lomonosov's MSU branch in Baku
Binagadi region, University str., 1, Hojasan, Baku

The photoluminescence spectra (PhL) $Ca_{0.5}Ba_{0.5}Ga_2S_4$, doped by rare-earth element atoms Eu and Er at 10÷300K are investigated. The radiation lines at 530nm are connected by transition $4f^65d\rightarrow4f^7(^8S_{7/2})$ of Eu^2 ion and transition $^4F_{9/2}\rightarrow{}^4I_{15/2}$ of Er^{3+}ion corresponds to wavelength interval 650÷675nm. The activation energies of luminescence centers at 0.1 and 0.16eV values are defined. Using value τ_e=291nsec one can evaluate the probability values of radiationless transition (A) which are equal to 10^7 sec^{-1} and 10^6 sec^{-1} for crystal.

Keywords: solid solutions, radiation spectrum, excitation, luminescence kinetics, the probability of radiationless transition.
PACS: 76.30., 78.55., 78.60.

INTRODUCTION

Last time the luminescence of rare-earth elements (REE) is intensively investigated in wide-band semiconductors [1-3]. This is caused by the fact that the effective excitation of REE by means of foundation wide absorption bands is possible in semiconductors that decreases the excitation threshold and moreover increases the luminescence efficiency. Besides, the study of spectral-luminescence properties of REE in semiconductors and dielectrics gives the more total information about nearest surrounding of REE, luminescence symmetry centers, crystal field etc.

The investigation of triple alkaline-earth chalcogenide semiconductors of $II\text{-}III_2\text{-}VI_4$ (II-Ca, Sr, Ba; III-Ga, Al; VI-S, Se, O) type activated by rare-earth ions are advanced ones. The investigated materials doped by Er^{3+}ion demonstrate the high-efficiency luminescence with decay time of several millisecond order being the promising one for usage in telecommunication in visualization aims and in laser techniques [4].

The values for damping time of emission peaks corresponding to levels $^4G_{11/2}$ and $^2H_{9/2}$ at wavelength λ_{ex} = 337.1nm and temperature 80 K for $CaGa_2S_4:Er^{3+}$ are given in [4]. The damping times for levels $^4G_{11/2}$ and $^2H_{9/2}$ are equal to 3,4 and 38μsec correspondingly. As it is known, REE ions can take three different positions corresponding to three different point symmetries in calcium ion exchange but indeed, Ln^{3+} ions can take only two different positions of Ca^{2+} calcium ions.

The contribution in these different centers can be more obvious one when the excitation takes place because of transitions on 4F levels of Er^{3+} ions than because of charge carrier transfer [5]. The radiation intensity of Eu^{2+} in dependence on Er^{3+} concentration is maximal at 5% Er^{3+}. It is shown that in interval 870-920nm ($^4S_{3/2}\rightarrow{}^4I_{13/2}$) the radiation intensity connected with Er^{3+} ions is also maximal one for 5% Er^{3+}. It is necessary to note that for λ_{ex}=337.1nm in interval 400-550nm, i.e. at 400nm ($H_{9/2}\rightarrow{}^4I_{15/2}$), 460nm ($^4F_{5/2}\rightarrow{}^4I_{15/2}$), 530nm ($^2H_{11/2}\rightarrow{}^4I_{15/2}$) and 550nm ($^4S_{3/2}\rightarrow{}^4I_{15/2}$) the radiation of Er^{3+} ion isn't observed [6].

The luminescence of many semiconductors and dielectric compounds activated by REE differs by big luminescence efficiency. The luminescence time interval (τ) is $10^{-4}\div10^{-2}$ sec. If the system contains more than one of REE then non-additive properties being the result of REE interaction can appear [7-10]. REE interaction is especially revealed in crystal phosphors at big concentrations.

Last time the investigations of properties of mixed compounds MGa_2S_4–$M'Ga_2S_4$(M=Ca,M'=Ba are alkaline-earth metals) activated by REE are carried out [12-14].

The analysis of literature review shows that compound of MGa_2S_4–$M'Ga_2S_4$ type isn't studied enough; the practical recommendations of these materials in the capacity of effective luminophors in visible spectrum region are absent. The investigation of radiation properties (radiation spectrum, excitation, luminescence kinetics of MGa_2S_4-$M'Ga_2S_4$ crystals) presents the significant interest.

SAMPLE SYNTHESIS AND EXPERIMENT TECHNIQUE.

In given work the binary components Ca(Ba)S and Ga_2S_3 are taken for synthesis of MGa_2S_4–$M'Ga_2S_4$ compounds.

The binary compounds BaS, CaS, Ga_2S_3 are put in quartz ampoule which is evacuated up to $10^{-4}\div10^{-5}$ millimeter of mercury and sealed. The activation by rare-earth Eu^{2+}, Er^{3+} ions is carried out by addition in mixture of synthesized solid solutions of $EuF_3$and ErF_3 compounds. The synthesis is carried out in evacuated quartz ampoule at 1000°C during one hour. After that the temperature gradually decreases up to 800°C and responded products are annealed during 10 hours after finishing of which the furnace is switched off and cooled towards with ampoule. The spectra of roentgenophase analysis are obtained on diffractometer D8 Advance

Diffractometer. The luminescence spectra are obtained on spectrometer HR-460 (Jobin-IvonSpectrometerHR 460). The helium-cadmium laser (HeCd) (325nm), UV light-emitting diode (367nm), laser diode (405nm), Nd^{3+}:YAG laser (325nm) and xenon lamp serve as excitation sources.

The excitation spectrum at room temperature of $Ca_{0.5}Ba_{0.5}Ga_2S_4$:Eu,Er crystal and radiation one in 10÷300K temperature interval are shown on fig.1 (a,b). As it is seen from fig.1b PhL intensity decreases with temperature increase. The maximum 530nm (2,34eV) which is caused by $4f^65d \rightarrow 4f^7(^8S_{7/2})$ transition of Eu^{2+} ions is observed in PhL spectrum of $Ca_{0.5}Ba_{0.5}Ga_2S_4$:Eu,Er in investigated temperature interval [15,16]. The introduction of erbium ions in $Ca_{0.5}Ba_{0.5}Ga_2S_4$:Eu^{2+} leads to appearance of weak peaks in PhL spectra of PhL lines in 650÷675 nm region which correspond to transitions $^4F_{9/2} \rightarrow {}^4I_{15/2}$ of Er^{3+} ions (fig.2).

At excitation by different wavelength waves 325, 367 and 405nm the radiation spectrum maximums of $Ca_{0.5}Ba_{0.5}Ga_2S_4$:Eu,Er luminophor don't depend on wavelengths of excitation light (fig.2). The maximum position place doesn't dependence on excitation wavelength (325, 367, 405nm) that evidences Eu^{2+} ion center transition.

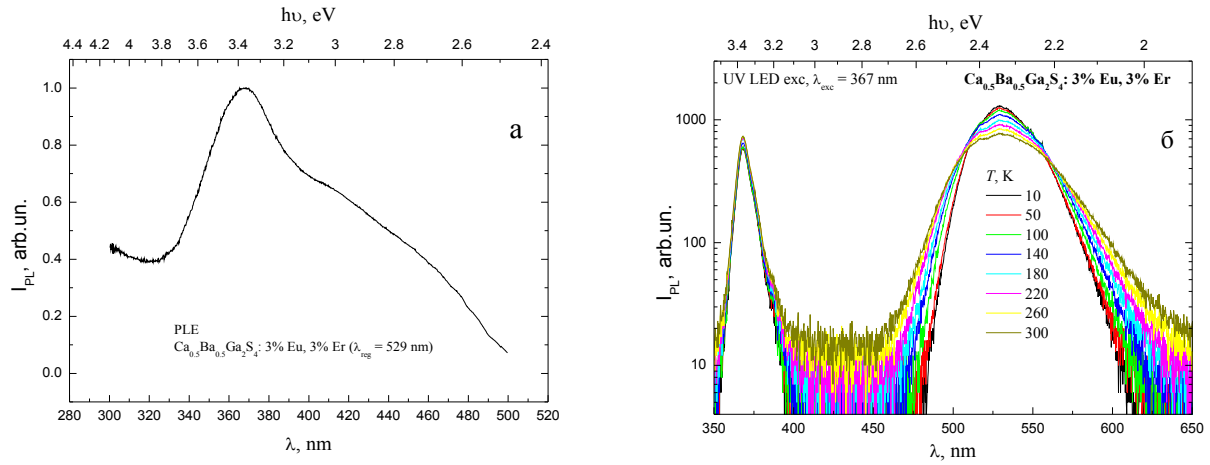

Fig. 1. PhL excitation spectrum at excitation by xenon lamp radiation at room temperature (a) and photoluminescence spectrum of $Ca_{0.5}Ba_{0.5}Ga_2S_4$:3%Eu,3%Er sample at temperatures 10÷300 K (b).

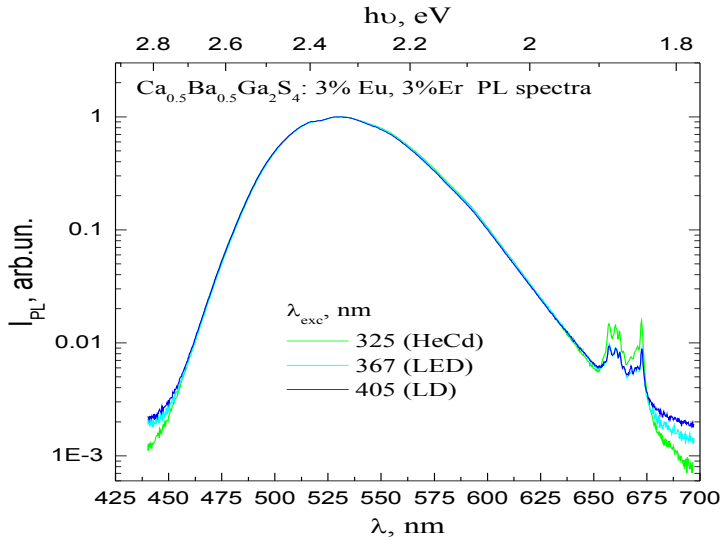

Fig.2. PhL spectra of $Ca_{0.5}Ba_{0.5}Ga_2S_4$:Eu,Er sample at excitation by HeCd laser continuous radiation (325nm), UV LED (367nm) and laser diode (405nm) at room temperature (normalized values on intensity).

The investigation results of PhL kinetics are sample excitation by impulse radiation on nanosecond time interval at room temperature are shown on fig.3. The increase of Ca concentration from 0,1 up to 0,5% in $Ca_xBa_{1-x}Ga_2S_4$ semiconductor matrix leads to increase of time τ_e of excitation state from 232 up to 291 nanosecond.

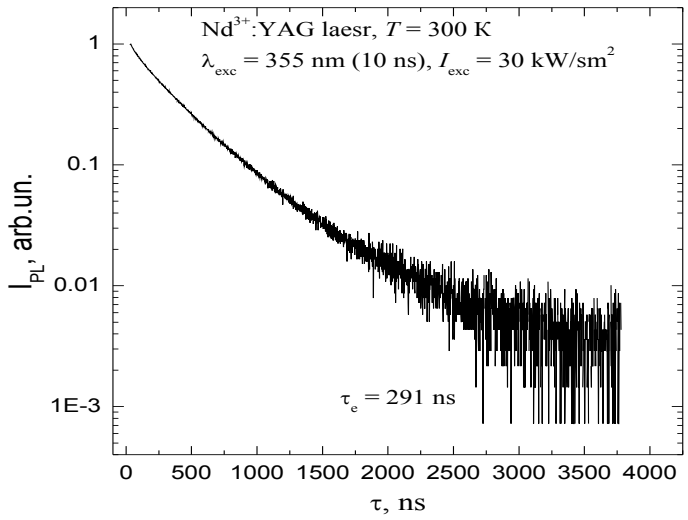

Fig. 3. PhL kinetics of investigated sample at excitation by impulse radiation 10 nanosecond time interval on wavelength 355 nm Nd^{3+}: laser YAG at room temperature (normalized values on intensity).

The radiation band intensity with maximum 530nm decreases with temperature increase and half-width decreases. The temperature dependence of maximums in PhL spectra of $Ca_{0.5}Ba_{0.5}Ga_2S_4$: Eu, Er is analysed by Mott formula [17] modified by authors [18]:

$$I = I_0 \frac{1}{1 + \tau_e A e^{\frac{\Delta E}{kT}}} \qquad (3.7)$$

Here I_0 is initial intensity where is the temperature quenching is absent, τ_e is mean lifetime of Eu^{2+} ion excitation state, A characterizes the probability radiationless transition, k is Boltzmann coefficient, T is absolute temperature, ΔE is quenching energy. The value A weakly depends on temperature whereas τ doesn't depend on temperature [18]. The formula (3.7) can be rewritten in the fillowing form:

$$\lg\left(\frac{I_0}{I} - 1\right) = \lg(\tau_e A) - \frac{0{,}43\Delta E}{kT} \qquad (3.8)$$

As it is seen from fig.4., the dependence of $\lg(I_0/I\text{-}1)$ on $10^3/T$ is linear one for $Ca_{0.5}Ba_{0.5}Ga_2S_4$:Eu,Er.

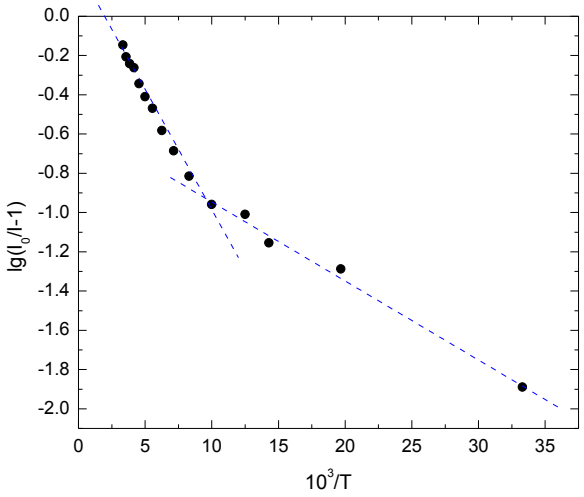

Fig.4. Temperature dependence of PhL intensity of $Ca_{0.5}Ba_{0.5}Ga_2S_4$:Eu,Er crystal.

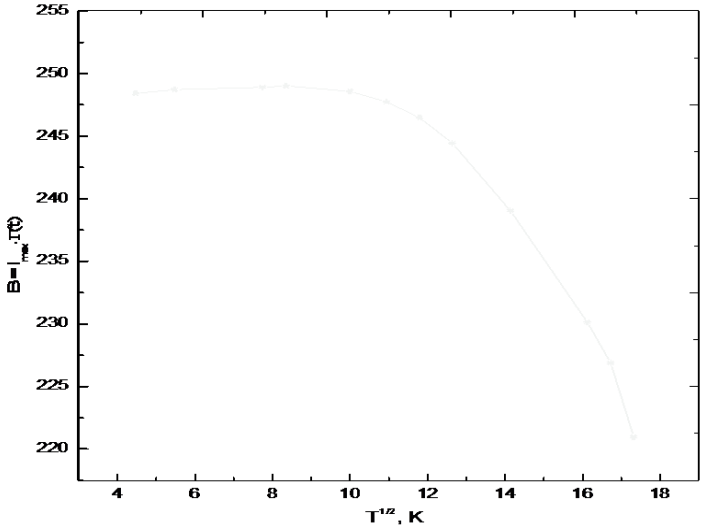

Fig. 5. Temperature dependence of radiation factum $I_{max}\cdot\Gamma(T)$ in PhL spectrum $Ca_{0.5}Ba_{0.5}Ga_2S_4$: Eu, Er

This dependence (fig.4.) has two linear parts to which corresponds the activation energies 0.10 and 0.16eV of traps taking part in luminescence process. The value of factum $\tau_e A_1$ and $\tau_e A_2$ which are equal to ~0,36 and -0,5 is evaluated by extrapolation of this two parts. Using the values τ_e=291 nsec one can evaluate values A_1 and A_2 for two parts which for investigated material are equal to A_1= 10^7 sec^{-1} and A_2=10^6 sec^{-1}.

The analysis of experimental data of half-width Γ(T) temperature dependences of $Ca_{0.5}Ba_{0.5}Ga_2S_4$:Eu,Er PhL spectrum shows that in 15÷100K interval the product of maximum intensities on half-width ($I_{max}\cdot\Gamma(T)$) almost doesn't depend on temperature. This is well illustrated on fig.5. The increase of $Ca_{0.5}Ba_{0.5}Ga_2S_4$:Eu,Er half-width PhL spectrum at temperature increase is expressed by model connected the formation of luminescence spectrum with phonon interaction process with matrix.

CONCLUSION

The analysis of obtained data shows that maximum in $Ca_{0.5}Ba_{0.5}Ga_2S_4$:Eu,Er PhL spectrum at 530nm is caused by $4f^65d\rightarrow 4f^7(^8S_{7/2})$ transition of Eu^{2+} ions and corresponds to $^4F_{9/2}\rightarrow{}^4I_{15/2}$ transion of Er^{3+} ions in interval of wavelengths 650÷675nm. The two parts are observed on $lg(I_0/I-1)\sim f(10^3)/T$ dependence that evidences about two trap levels with activation energy 0.10 and 0.16eV taking part in luminescence process. Using the value τ_e one can evaluate A values, which are equal to A_1=10^7 sec^{-1} and A_2=10^6 sec^{-1} for crystal. It is established that in temperature interval the product $I_{max}\cdot\Gamma(T)$=const.

The given work has been supported by Science Development Foundation under the President of the Republic of Azerbaijan – Grant № EIF-BGM-2-BRFTF-1-2012/2013-07/02/1.

[1] *T. Jeremy Anderson.* Luminescent Sulfides and Solution-Deposited Oxide Thin Films // Dissertation, 2008.

[2] A.*N. Qeorqobiani, B.Q. Taqiev, Q.Q. Quseynov, T.Q. Kerimova, O.B. Taqiev, S.Q. Asadullaeva.* Osobennosti strukturi I fotolyumineschenchiya soedineniya $ZnGa_2Se_4$:Eu // Неорганические материалы, 2010, т. 46, №5, с.524-527.

[3] *A.N. Georgobiani, V.V. Styrov, V.I. Tyutyunnikov, B.G. Tagiev, O.B. Tagiev, R.B. Djabbarov*. Radical-recombination luminescence, ion-luminescence and photoluminescence of $CaGa_2S_4$:Eu. //Journal of Physics and Chemistry of Solids. 2003, v. 64, Issues 9-10, p. 1519-1524.

[4] *A. Garcia, F. Guillen, C. Fouassier*. Charge transfer excitation of the Nd^{3+}, Sm^{3+}, Dy^{3+}, Ho^{3+}, Er^{3+} and Tm^{3+} emission in $CaGa_2S_4$ // J. of Luminescence. 1985, v.33, p. 15-27.

[5] *A. Eisenmann, M. Jakowski, Klee W., Shäfer H. Die*. Strukturen von $CaAl_2S_4$, $CaGa_2S_4$, $SrGa_2S_4$, $SrGa_2S_4$ und $BaIn_2S_4$ // Revue de Chimie Minérale. 1983, v.20, No 2, p. 255-263.

[6] *A. Barthou, P. Benolloul, B.G. Tagiev, O.B. Tagiev, S.A. Abushov, F.A. Kazimova, A.N. Georgobiani.* Energy transfers between Eu^{2+} and Er^{3+} in $EuGa_2S_4$:Er^3 // J.Phys.: Condens. Matter. 2004. №16, 8075-8084.

[7] *J. Choi, S. Baek, S. Kim, S. Lee, H. Park.* Energy transfer between Ce^{3+} and Eu^{2+} in $SrAl_{12}O_{19}$:Ce_x^{3+}, $Eu_{0.01}{}^{2+}$ (x=0.01-0.09) // Material Research Bulletin, 1999, v.34, No.4, p.551-556.

[8] *H. Jeon, S. Kim, H. Park, G. Kim.* Observation of Two Independent Energy Transfer Mechanisms in $BaAl_{12}O_{19}$:Ce^{3+}+Eu^{2+} phosphor //Solid State Communications, 2001, v. 120, p. 221-225.

[9] *H. Jeon, S. Kim, T. Kim, S. Chang*. Energy transfer mechanisms in $CaAl_{12}O_{19}:Ce_{0.06}^{3+}$, Eu_x^{2+} phosphors // Materials Research Bulletin, 2000, v.35, p.1447-1452.

[10] *H. Lin, X. Liu, E. Pun*. Sensitized luminescence and energy transfer in Ce^{3+} and Eu^{2+}codoped calcium magnesium chlorosilicate // Optical Materials, 2002, v.18, p.397-401.

[11] *T. Peters, J. Baglio*. Luminescence and Structural Properties of Thiogallate Ce^{3+} and Eu^{2+}activated Phosphors //J. Electrochem. Soc. 1972, v.119, No2, p.230-236.

[12] *Ki-Young Ko, Young-Duk Huh, and Young Rag Do.* Cathodoluminescenceand Longevity Properties of Potential $Sr_{1-x}M_xGa_2S_4$:Eu (M = Ba or Ca) Green Phosphors for Field Emission DisplaysBull// Korean Chem. *Soc*. 29 (2008**)** 822–826.

[13] *Ruijin Yu, Jing Wang, Mei Zhang, Haibin Yuan, WeijiaDing,Yun An, and Qiang Su.* Luminescence Properties of $Ca_{1-x}Sr_x(Ga_{1-y}Al_y)_2S_4:Eu^{2+}$ and Their Potential Application for White LEDs // Journal of The Electrochemical Society, 155 (10) J290-J292 (2008).

[14] *Chiharu Hidaka, EriYamagishi, Takeo Takizawa.* Preparation of $Ca_{1-x}Eu_xGa_2S_4$crystals and their photoluminescence, absorption and excitation spectra // Journal of Physics and Chemistry of Solids, 01/2005; 66(11), 2058-2060.

[15] *P. Dorenbos.* Energy of the first $4f^7 \rightarrow 4f^65d$ transition of Eu^{2+} in inorganic compounds // J. of Luminescence, 2003, v. 104, p. 239-260.

[16] *B. Tagiev, R. Jabbarov, C. Chartier et al.* Radiative properties of Eu^{2+} $BaGa_2S_4$ // J. Phys. Chem. Sol., 2005, v. 66, No 6, p. 1049–1056.

[17] *N. Mott, R. Gurney*. Electronic processes in ionic crystals. Oxford 1948, p. 231–234.

[18] *B.B. Antonov-Romanskiy*. Kinetika fotolyumineschenchii kristallofos-forov. M.: Nauka, 1966, 324 s.

Recevied: 02.05.2014

HIGGS BOSON PRODUCTION IN ELECTRON-POSITRON SCATTERING

S.Q. ABDULLAYEV, M.S. GOJAYEV, F.A. SADDIGH
Baku State University, AZ-1148, Z.Khalilov, 23, Baku, Azerbaijan
s_abdullayev@mail.ru, m_qocayev@mail.ru, f_seddig@yahoo.com

In the framework of Standard Model the process of scalar Higgs boson production in electron-positron scattering has been investigated: $e^-e^+ \Rightarrow He^-e^+$. It is shown that, the annihilation (scattering) diagram is defined by only four helisity amplitudes $F_{LL}^{(a)}$, $F_{LR}^{(a)}$, $F_{RL}^{(a)}$ and $F_{RR}^{(a)}$ ($F_{LR}^{(s)}$, $F_{RL}^{(s)}$, $F_{LL}^{(s)}$ and $F_{RR}^{(s)}$), which describe following reactions: $e_L^-e_R^+ \Rightarrow He_L^-e_R^+$, $e_L^-e_R^+ \Rightarrow He_R^-e_L^+$, $e_R^-e_L^+ \Rightarrow He_L^-e_R^+$ and $e_R^-e_L^+ \Rightarrow He_R^-e_L^+$ ($e_L^-e_R^+ \Rightarrow He_L^-e_R^+$, $e_R^-e_L^+ \Rightarrow He_R^-e_L^+$, $e_L^-e_L^+ \Rightarrow He_L^-e_L^+$ and $e_R^-e_R^+ \Rightarrow He_R^-e_R^+$). The cross-sections are calculated for spiral processes and analytic expressions are obtained. At the energy $\sqrt{s} = 500$ GeV the distributions of Higgs boson over angles and energy are studied.

Keywords: Higgs boson, left and right coupling constants, spirality, Weinberg's parameter, helicity amplitudes.
PACS: 12.38.Bx, 12.38.Cy, 13.66.

INTRODUCTION

The Weinberg Salam unified theory of Electromagnetic and weak interaction (Standard Model – SM) has achieved great success [1]. It includes the production of neutral weak current, discovery of $W^{\pm}$- and Z^0-gauge bosons and some of its claims are investigated successfully in experiments. One of the important acclaims of SM is the prediction for the existence of scalar Higgs boson. Some experiments are carried out for the discovery of Higgs boson in different Experimental Labs.

Finally in Tevatron and CERN new information are received concerning the existence of Higgs boson with the mass of 125 GeV [2-7]. So the channels which give rise to Higgs bosons have got more attentions [8-10].

In this work scattering of e^-e^+ with longitudinal polarization is studied for the sake of production of Higgs boson:

$$e^- + e^+ \to H + e^- + e^+ . \qquad (1)$$

The Feynman diagrams for the process (1) shown in fig. 1 (the momentum and helicity of the particles are shown in parentheses). First diagram is the annihilation diagram i.e. e^-e^+-pairs first annihilate to Z^0-boson and Z^0 in turn transforms to e^-e^+-pair while releasing Higgs boson. The diagram of scattering that is shown in fig. 1 can describe the process as follow: both electron and positron release Z^0-boson while being scattered and these bosons create Higgs boson.

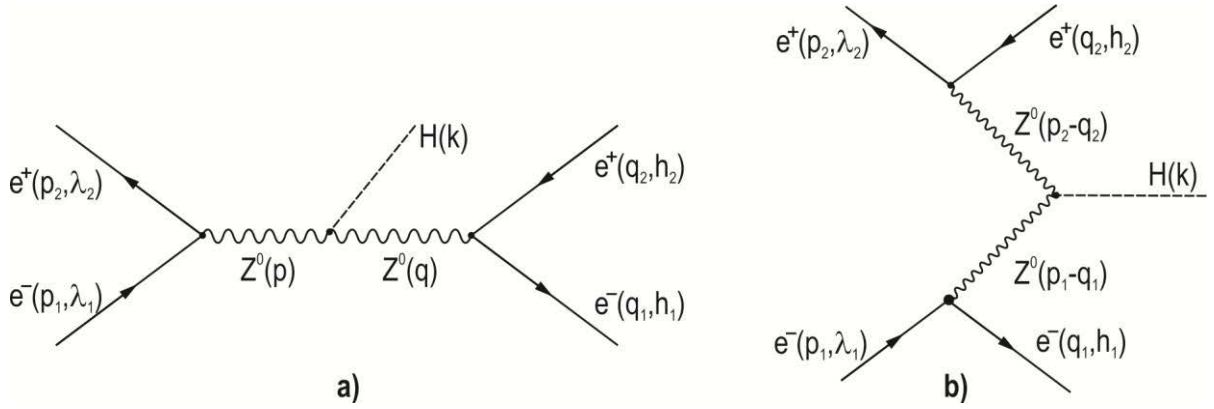

Fig 1. Feynman diagrams for $e^-e^+ \to He^-e^+$

As we know the Lagrangian for interaction of fermions with Z^0-boson and Z^0-boson with Higgs boson can be written as follow [1]:

$$L_{eeZ} = \frac{e}{2\sin\theta_w.\cos\theta_w}[g_L\bar{e}\gamma_\mu(1+\gamma_5)e + g_R\bar{e}\gamma_\mu(1-\gamma_5)e]Z_\mu, \qquad (2)$$

$$L_{ZZH} = \frac{eM_Z}{2\sin\theta_w.\cos\theta_w} Z_\mu Z_\rho g_{\mu\rho} H(k),$$

Here

$$g_L = -\frac{1}{2} + \sin^2\theta_w, \qquad g_R = \sin^2\theta_w \tag{3}$$

- are the constants for interaction of right and left handed electrons with Z^0-boson, θ_W – is the Weinberg's angle.

According to the Lagrangian given in (2) for the diagram (a) we can write the following transition amplitude:

$$M_a(e^-e^+ \to He^-e^+) = \left(\frac{e}{2\sin\theta_W\cos\theta_W}\right)^3 M_Z \overline{\upsilon}(p_2, \lambda_2)\gamma_\mu[g_L(1+\gamma_5) + g_R(1-\gamma_5)]\times$$
$$\times u(p_1, \lambda_1) D_{\mu\rho}(p) D_{\rho\nu}(q)\overline{u}(q_1, h_1)\gamma_\nu[g_L(1+\gamma_5) + g_R(1-\gamma_5)]\upsilon(q_2, h_2), \tag{4}$$

Here

$$D_{\mu\rho}(p) = \left(-g_{\mu\rho} + \frac{p_\mu p_\rho}{M_Z^2}\right).\frac{1}{p^2 - M_Z^2 + iM_Z\Gamma_Z} \tag{5}$$

– is the propagator of Z^0-boson, $p = p_1 + p_2$, $q = q_1 + q_2 = p - k$, and M_Z and Γ_Z signifies the mass and total width of Z^0 boson.

At high energies we can neglect the mass of electron which will cause in conservation of weak currents:

$$(p_1 + p_2)_\mu \overline{\upsilon}(p_2, \lambda_2)\gamma_\mu[g_L(1+\gamma_5) + g_R(1-\gamma_5)]u(p_1, \lambda_1) = 0,$$
$$(q_1 + q_2)_\nu \overline{u}(q_1, h_1)\gamma_\nu[g_L(1+\gamma_5) + g_R(1-\gamma_5)]\upsilon(q_2, h_2) = 0.$$

This will make the amplitude (4) to take a simpler form:

$$M_a(e^-e^+ \to He^-e^+) = \left(\frac{e}{2\sin\theta_W\cos\theta_W}\right)^3 \cdot M_Z \cdot D_Z(s)\cdot D_Z(xs)\overline{\upsilon}(p_2, \lambda_2)\times$$
$$\times\gamma_\mu[g_L(1+\gamma_5) + g_R(1-\gamma_5)]u(p_1, \lambda_1)\overline{u}(q_1, h_1)\gamma_\mu[g_L(1+\gamma_5) + g_R(1-\gamma_5)]\upsilon(q_2, h_2). \tag{6}$$

Here s – is the square of total sum of energies of electron and positron in the center of mass frame and

$$D_Z(s) = (s - M_Z^2 + iM_Z\Gamma_Z)^{-1}, \quad x = 1 - \frac{2\omega}{\sqrt{s}} + \frac{M_H^2}{s}, \tag{7}$$

where M_H and ω are the mass and energy of Higgs boson.

2. Helicity is conserved at high energy. The conservation of helicity imply that electron and positron colliding at the same vertex to have opposite helicities: $e_L^- e_R^+$ or $e_R^- e_L^+$. Here e_L^- (e_R^+) – is the electron (positron) with left (right) helicity. So, four helicity amplitudes will correspond to the diagram (a): $F_{LL}^{(a)}$, $F_{LR}^{(a)}$, $F_{RL}^{(a)}$ and $F_{RR}^{(a)}$ (first and second indices indicate the initial and final helicity of electron). These helicity amplitudes are given by following expressions:

$$F_{LL}^{(a)} = D_Z(s)D_Z(xs)g_L^2, \qquad F_{LR}^{(a)} = D_Z(s)D_Z(xs)g_L g_R,$$
$$F_{RL}^{(a)} = D_Z(s)D_Z(xs)g_R g_L, \quad F_{RR}^{(a)} = D_Z(s)D_Z(xs)g_R^2. \tag{8}$$

And correspondingly they describe the following process:

$$e_L^- + e_R^+ \Rightarrow H + e_L^- + e_R^+, \quad e_L^- + e_R^+ \Rightarrow H + e_R^- + e_L^+,$$
$$e_R^- + e_L^+ \Rightarrow H + e_L^- + e_R^-, \quad e_R^- + e_L^+ \Rightarrow H + e_R^- + e_L^+$$

Let's first calculate the square of amplitude for the process $e_L^- + e_R^+ \Rightarrow H + e_L^- + e_R^+$:

$$M_a(e_L^- e_R^+ \Rightarrow H e_L^- e_R^+) = \left(\frac{e}{2\sin\theta_W \cos\theta_W}\right)^3 M_Z \cdot F_{LL}^{(a)}[\overline{\upsilon}(p_2,\, \lambda_2 = 1)\times$$
$$\times \gamma_\mu(1+\gamma_5)u(p_1,\, \lambda_1 = -1)][\overline{u}(q_1, h_1 = -1)\gamma_\mu(1+\gamma_5)\upsilon(q_2,\, h_2 = 1)],$$
$$M_a^+(e_L^- e_R^+ \Rightarrow H e_L^- e_R^+) = \left(\frac{e}{2\sin\theta_W \cos\theta_W}\right)^3 \cdot M_Z \cdot F_{LL}^{*(a)}[\overline{u}(p_1,\, \lambda_1 = -1)\times$$
$$\times \gamma_\nu(1+\gamma_5)\overline{\upsilon}(p_2,\, \lambda_2 = 1)][\overline{\upsilon}(q_2, h_2 = 1)\gamma_\nu(1+\gamma_5)u(q_1,\, h_1 = -1)],$$
$$|\, M_a(e_L^- e_R^+ \Rightarrow H e_L^- e_R^+)\,|^2 = \left(\frac{e^2}{4x_w(1-x_w)}\right)^3 \cdot M_Z^2 \cdot |\, F_{LL}^{(a)}\,|^2 \cdot T_{\mu\nu}^{(1)} \cdot T_{\mu\nu}^{(2)}. \qquad (9)$$

Here $x_w = \sin^2\theta_w$ is the Weinberg's parameter while $T_{\mu\nu}^{(1)}$ and $T_{\mu\nu}^{(2)}$ are the tensors of 4-momentum for initial and final pair of $e^- e^+$:

$$T_{\mu\nu}^{(1)} = tr[\upsilon(p_2,\, \lambda_2 = 1)\overline{\upsilon}(p_2,\, \lambda_2 = 1)\gamma_\mu(1+\gamma_5)u(p_1,\, \lambda_1 = -1)\times$$
$$\times \overline{u}(p_1, \lambda_1 = -1)\gamma_\nu(1+\gamma_5)] = tr\left[\frac{1}{2}(1+\gamma_5)\hat{p}_2\gamma_\mu(1+\gamma_5).\frac{1}{2}(1+\gamma_5)\hat{p}_1\gamma_\nu(1+\gamma_5)\right] =$$
$$= 8[p_{1\mu}p_{2\nu} + p_{2\mu}p_{1\nu} - (p_1.p_2)g_{\mu\nu} - i\varepsilon_{\mu\nu\rho\sigma}p_{1\rho}p_{2\sigma}], \qquad (10)$$
$$T_{\mu\nu}^{(2)} = tr[u(q_1,\, h_1 = -1)\overline{u}(q_1,\, h_1 = -1)\gamma_\mu(1+\gamma_5)\upsilon(q_2,\, h_2 = 1)\times$$
$$\times \overline{\upsilon}(q_2, h_2 = 1)\gamma_\nu(1+\gamma_5)] = tr\left[\frac{1}{2}(1+\gamma_5)\hat{q}_1\gamma_\mu(1+\gamma_5).\frac{1}{2}(1+\gamma_5)\hat{q}_2\gamma_\nu(1+\gamma_5)\right] =$$
$$= 8[q_{1\mu}q_{2\nu} + q_{2\mu}q_{1\nu} - (q_1.q_2)g_{\mu\nu} + i\varepsilon_{\mu\nu\alpha\beta}q_{1\alpha}p_{2\beta}]\cdot \qquad (11)$$

The product of two tensors $T_{\mu\nu}^{(1)}$ and $T_{\mu\nu}^{(2)}$ is a simple relation:

$$T_{\mu\nu}^{(1)} \cdot T_{\mu\nu}^{(2)} = 2^8(p_1 \cdot q_2)(p_2 \cdot q_1). \qquad (12)$$

So, the square amplitude of the process $e_L^- + e_R^+ \Rightarrow H + e_L^- + e_R^+$ will be equal to:

$$|\, M_a(e_L^- e_R^+ \Rightarrow H e_L^- e_R^+)\,|^2 = 4\left(\frac{e^2}{x_w(1-x_w)}\right)^3 M_Z^2 .|\, F_{LL}^{(a)}\,|^2 .(p_1.q_2)(p_2.q_1). \qquad (13)$$

Because of conservation of helicity no interference will happen between the of different annihilation diagrams. So, we easily will be able to calculate the square of amplitudes for other helicity processes:

$$|M_a(e_L^-e_R^+ \Rightarrow He_R^-e_L^+)|^2 = 4\left(\frac{e^2}{x_w(1-x_w)}\right)^3 .M_Z^2 .|F_{LR}^{(a)}|^2 (p_1.q_1)(p_2.q_2),$$

$$|M_a(e_L^-e_R^+ \Rightarrow He_L^-e_R^+)|^2 = 4\left(\frac{e^2}{x_w(1-x_w)}\right)^3 .M_Z^2 .|F_{RL}^{(a)}|^2 (p_1.q_1)(p_2.q_2), \quad (14)$$

$$|M_a(e_R^-e_L^+ \Rightarrow He_R^-e_L^+)|^2 = 4\left(\frac{e^2}{x_w(1-x_w)}\right)^3 .M_Z^2 .|F_{RR}^{(a)}|^2 (p_1.q_2)(p_2.q_1).$$

3. So, now we are ready to calculate the contributions coming from diagram (b). Let's write the matrix element for this piece:

$$M_b(e^-e^+ \Rightarrow He^-e^+) = -\left(\frac{e}{2\sin\theta_W \cos\theta_W}\right)^3 M_Z \times$$

$$\times \{F_{LR}^{(s)}[\bar{u}(q_1, h_1)\gamma_\mu(1+\gamma_5)u(p_1, \lambda_1)][\bar{\upsilon}(p_2, \lambda_2)\gamma_\mu(1+\gamma_5)\upsilon(q_2, h_2)] +$$

$$+ F_{LL}^{(s)}[\bar{u}(q_1, h_1)\gamma_\mu(1+\gamma_5)u(p_1, \lambda_1)][\bar{u}(p_2, \lambda_2)\gamma_\mu(1-\gamma_5)\upsilon(q_2, h_2)] +$$

$$+ F_{RR}^{(s)}[\bar{u}(q_1, h_1)\gamma_\mu(1-\gamma_5)u(p_1, \lambda_1)][\bar{u}(p_2, \lambda_2)\gamma_\mu(1+\gamma_5)\upsilon(q_2, h_2)] +$$

$$+ F_{RL}^{(s)}[\bar{u}(q_1, h_1)\gamma_\mu(1-\gamma_5)u(p_1, \lambda_1)][\bar{u}(p_2, \lambda_2)\gamma_\mu(1-\gamma_5)\upsilon(q_2, h_2)]\}, \quad (15)$$

Here

$$\begin{aligned} F_{LR}^{(s)} &= D_Z(p_1-q_1)D_Z(p_2-q_2)g_L^2, & F_{RL}^{(s)} &= D_Z(p_1-q_1)D_Z(p_2-q_2)g_R^2, \\ F_{LL}^{(s)} &= D_Z(p_1-q_1)D_Z(p_2-q_2)g_Lg_R, & F_{RR}^{(s)} &= D_Z(p_1-q_1)D_Z(p_2-q_2)g_Rg_L \end{aligned} \quad (16)$$

are the helicity amplitudes for scattering diagram where the first and second index indicate the spiralities initial (final) electron and positron and:

$$D_Z(p_1-q_1) = [(p_1-q_1)^2 - M_Z^2]^{-1}$$

We see clearly from (15) that there are four helicity processes (the helicity will be conserved in each vertex of the scattering diagram):

1) Electron is polarized left-handed while positron is right-handed:

$e_L^- + e_R^+ \Rightarrow H + e_L^- + e_R^+;$

2) Both electron and positron are right handed

$e_L^- + e_L^+ \Rightarrow H + e_L^- + e_L^+;$

3) Both electron and positron are left handed

$e_R^- + e_R^+ \Rightarrow H + e_R^- + e_R^+;$

4) Electron is right-handed and positron is left-handed:

$e_R^- + e_L^+ \Rightarrow H + e_R^- + e_L^-;$

The interference will not occur between these amplitudes so the square of corresponding helicity processes will be given by the following relations:

$$
\begin{aligned}
|M_b(e_L^- e_R^+ \Rightarrow H e_L^- e_R^+)|^2 &= 4\left(\frac{e^2}{x_w(1-x_w)}\right)^3 \cdot M_Z^2 \cdot |F_{LR}^{(s)}|^2 (p_1.q_2)(p_2.q_1),\\
|M_b(e_L^- e_L^+ \Rightarrow H e_L^- e_L^+)|^2 &= 4\left(\frac{e^2}{x_w(1-x_w)}\right)^3 \cdot M_Z^2 \cdot |F_{LL}^{(s)}|^2 (p_1.p_2)(q_1.q_2),\\
|M_b(e_R^- e_R^+ \Rightarrow H e_R^- e_R^+)|^2 &= 4\left(\frac{e^2}{x_w(1-x_w)}\right)^3 \cdot M_Z^2 \cdot |F_{RR}^{(s)}|^2 (p_1.p_2)(q_1.q_2),\\
|M_b(e_R^- e_L^+ \Rightarrow H e_R^- e_L^+)|^2 &= 4\left(\frac{e^2}{x_w(1-x_w)}\right)^3 \cdot M_Z^2 \cdot |F_{RL}^{(s)}|^2 (p_1.q_2)(p_2.q_1).
\end{aligned}
\tag{17}
$$

It is interesting that the interference occur only between $e_L^- + e_R^+ \Rightarrow H + e_L^- + e_R^+$ and $e_R^- + e_L^+ \Rightarrow H + e_R^- + e_L^+$ and we then have:

$$
\begin{aligned}
|M_{\text{int}}(e_L^- e_R^+ \Rightarrow H e_L^- e_R^+)|^2 &= 8\left(\frac{e^2}{x_w(1-x_w)}\right)^3 \cdot M_Z^2\, \text{Re}[F_{LL}^{*(a)} F_{LR}^{(s)}] \cdot (p_1.q_2)(p_2.q_1),\\
|M_{\text{int}}(e_R^- e_L^+ \Rightarrow H e_R^- e_L^+)|^2 &= 8\left(\frac{e^2}{x_w(1-x_w)}\right)^3 \cdot M_Z^2\, \text{Re}[F_{RR}^{*(a)} F_{RL}^{(s)}] \cdot (p_1.q_2)(p_2.q_1)
\end{aligned}
\tag{18}
$$

So, we find out that only the following reactions have non-zero helicity amplitudes:

$$e_L^- + e_R^+ \Rightarrow H + e_L^- + e_R^+, \;\; e_R^- + e_L^+ \Rightarrow H + e_R^- + e_L^+, \tag{19}$$

$$e_L^- + e_R^+ \Rightarrow H + e_R^- + e_L^+, \;\; e_R^- + e_L^+ \Rightarrow H + e_L^- + e_R^+, \tag{20}$$

$$e_L^- + e_L^+ \Rightarrow H + e_L^- + e_L^+, \;\; e_R^- + e_R^+ \Rightarrow H + e_R^- + e_L^+. \tag{21}$$

It is clear that the reactions (19) is for both annihilation and scattering while (20) is only a reaction of annihilation and (21) is only contributing for scattering diagram. The square of the amplitudes of those transitions will be equal to:

$$
\begin{aligned}
|M(e_L^- e_R^+ \Rightarrow H e_L^- e_R^+)|^2 &= 4\left(\frac{e^2}{x_w(1-x_w)}\right)^3 \cdot M_Z^2 \cdot |F_{LL}^{(a)} + F_{LR}^{(s)}|^2 (p_1.q_2)(p_2.q_1),\\
|M(e_R^- e_L^+ \Rightarrow H e_R^- e_L^+)|^2 &= 4\left(\frac{e^2}{x_w(1-x_w)}\right)^3 \cdot M_Z^2 \cdot |F_{RR}^{(a)} + F_{RL}^{(s)}|^2 (p_1.q_2)(p_2.q_1),\\
|M(e_L^- e_R^+ \Rightarrow H e_R^- e_L^+)|^2 &= 4\left(\frac{e^2}{x_w(1-x_w)}\right)^3 \cdot M_Z^2 \cdot |F_{LR}^{(a)}|^2 (p_1.q_1)(p_2.q_2),\\
|M(e_R^- e_L^+ \Rightarrow H e_L^- e_R^+)|^2 &= 4\left(\frac{e^2}{x_w(1-x_w)}\right)^3 \cdot M_Z^2 \cdot |F_{RL}^{(a)}|^2 (p_1.q_1)(p_2.q_2),
\end{aligned}
\tag{22}
$$

$$|M(e_L^- e_L^+ \Rightarrow He_L^- e_L^+)|^2 = 4\left(\frac{e^2}{x_w(1-x_w)}\right)^3 \cdot M_Z^2 \cdot |F_{LL}^{(s)}|^2 (p_1.p_2)(q_1.q_2),$$

$$|M(e_R^- e_R^+ \Rightarrow He_R^- e_R^+)|^2 = 4\left(\frac{e^2}{x_w(1-x_w)}\right)^3 \cdot M_Z^2 \cdot |F_{RR}^{(s)}|^2 (p_1.p_2)(q_1.q_2).$$

4. The differential cross-section of each of the spiral process is proportional to the square of amplitude. We can calculate the effect of the distribution of final angle and energy for the Higgs boson by integrating over the momentum of final electron and positron pair. Generally the derived equations are very complicated, so at the range of resonance of Z^0 i.e. $xs = M_Z^2$ we will calculate and discuss the differential cross-section for the process $e^- + e^+ \to H + e^- + e^+$. In this range the contribution coming from the annihilation diagram is way above the scattering part by order of magnitude and when the initial pair is longitudinally polarized then the cross-section could be written as follow:

$$d\sigma = \frac{\alpha^3 s}{24\pi x_w^3 (1-x_w)^3} \cdot \frac{1}{(s-M_Z^2)^2} \cdot \frac{1}{\Gamma_Z^2} \cdot f(\omega,\theta)\sqrt{\omega^2 - M_H^2}\, d\omega d\Omega \times$$
$$\times [(1-\lambda_1)(1+\lambda_2)g_L^2 + (1+\lambda_1)(1-\lambda_2)g_R^2](g_L^2 + g_R^2), \qquad (23)$$

Here:

$$f(\omega,\theta) = 2x + \frac{1}{s}(\omega^2 - M_H^2)\sin^2\theta,$$

and θ is the angle between the momentums of initial electrons and Higgs bosons.

We see clearly from the relation (23) that the processes $e_L^- + e_R^+ \to H + e^- + e^+$ and $e_R^- + e_L^+ \to H + e^- + e^+$ have different cross-section from each other, so the left-right spin asymmetry for the reaction $e^- + e^+ \to H + e^- + e^+$ is not zero:

$$A_{LR} = \frac{d\sigma(e_L^- e_R^+ \to He^- e^+) - d\sigma(e_R^- e_L^+ \to He^- e^+)}{d\sigma(e_L^- e_R^+ \to He^- e^+) + d\sigma(e_R^- e_L^+ \to He^- e^+)} = \frac{g_L^2 - g_R^2}{g_L^2 + g_R^2}. \qquad (24)$$

This asymmetry gives the value of 14% when the Weinberg parameter x_w is equal to 0.232.

The distribution of Higgs boson over the angle and energy is given by following relation:

$$\frac{d\sigma}{d\omega d\Omega} = \frac{\alpha^3 s}{24\pi x_w^3 (1-x_w)^3} \cdot \frac{1}{(s-M_Z^2)^2} \cdot \frac{(g_L^2 + g_R^2)^2}{\Gamma_Z^2} \cdot f(\omega,\theta)\sqrt{\omega^2 - M_H^2}, \qquad (25)$$

$$\frac{d\sigma}{d\omega} = \frac{\alpha^3 s}{3x_w^3 (1-x_w)^3} \cdot \frac{(g_L^2 + g_R^2)^2}{(s-M_Z^2)^2} \cdot \frac{1}{\Gamma_Z^2} \cdot \left[1 - \frac{2\omega}{\sqrt{s}} + \frac{1}{3}(\omega^2 + 2M_H^2)\right]\sqrt{\omega^2 - M_H^2}, \qquad (26)$$

In the Fig. 2 the distribution of Higgs boson is being depicted over the angles for the energy $\sqrt{s} = 500$ GeV. Mass of the Higgs boson is 125 GeV and the Weinberg parameter (x_w) is chosen to be 0.232. We see from the diagram that the cross-section increase as the value of θ increase and at the θ=90^0 reaches to its maximum, by further increase in the value of parameter θ it starts to decrease.

In resonance range the cross-section $\frac{d\sigma\sqrt{s}}{d\omega}$ for the process $e^- + e^+ \to H + e^- + e^+$ is depicted over the mass of Higgs boson in the third figure. As the mass of Higgs boson increase the cross-section decrease. The cross-section is of order of 1,68 picobarn when $M_H = 125$ GeV.

CONCLUSION

The cross-section we get for $e_L^- + e_R^+ \Rightarrow H + e^- + e^+$ is different than what we get for $e_R^- + e_L^+ \Rightarrow H + e^- + e^+$ i. e. the left-right asymmetry should be observed.

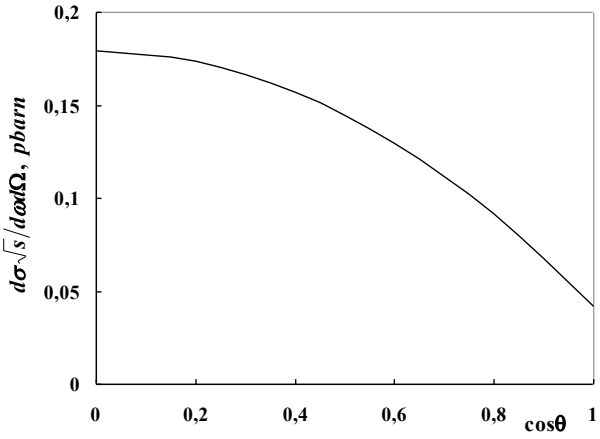

Fig 2. The cross-section $\frac{d\sigma\sqrt{s}}{d\omega d\Omega}$ for the reaction $e^-e^+ \to He^-e^+$ as a function of $\cos\theta$.

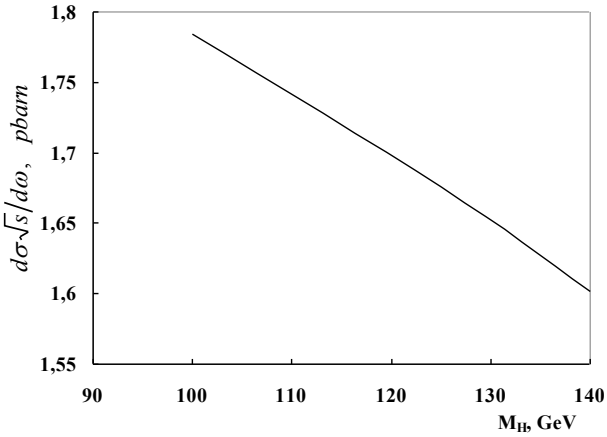

Fig 3. The cross-section $\frac{d\sigma\sqrt{s}}{d\omega}$ for the reaction $e^-e^+ \to He^-e^+$ as a function of M_H.

As the angle of outgoing Higgs boson increase, the cross-section also increases and reaches to its maximum at the value of $\theta = 90°$. Bu further increase of angle the cross-section starts to decrease.

By increasing the Higgs boson mass the cross-section will be decreased.

[1] *S.Q. Abdullayev.* Lepton-lepton və lepton-hadron qarşılıqlı təsirlərində zəif cərəyan effektləri (I-Hissə). Bakı, 2012, «AM965 MMC» nəşriyyatı, 484 səh.

[2] ATLAS Collaboration. Observation of a new particle in the search for the standard model Higgs boson with the ATLAS detector at the LHC // Phys. Lett. B, 2012, V.716, p.1-29.

[3] CDF Collaboration, Aaltonen T., et al. Phys. Rev. Lett. (2012), in press, arxiv: 1207.1707 [hep-ex].

[4] DF Collaboration, Abazov V.M. et al. Phys. Rev. Lett. (2012), submitted for publication, arxiv: 1207.6631 [hep-ex].

[5] CDF Collaboration, Do Collaboration, Phys. Rev. Lett. (2012), submitted for publication, arxiv: 1207.6436 [hep-ex].

[6] ATLAS Collaboration, Phys. Rev. D 86 (2012) 032003.

[7] CMS Collaboration, Phys. Lett. B 710 (2012) 26.

[8] *D.De Florian, M. Grazzini.* Higgs pro$\sqrt{s}$duction at the LHC: Updated cross-sections at 8 TeV, arxiv: 1207.6436 [hep-ex].

[9] *D.De Florian, G. Ferrera, M. Grazzini, D. Tommasini*. JHEP 1111, 2011, 064.

[10] *S. Dittmaier, C. Mariotti, G. Passarino, R. Tanaca.* LHC Higgs Cross-section Working Group, Handbook of LHC Higgs cross-sections: 1. Inclusive observables, CERN-2011-002, arxiv: 1101.0593 [hep-pn], 2011; 2. Differential Distributions, CERN-2011-002, arxiv: 1201.3084 [hep-pn], 2012.

Recevied: 16.09.2014

ISSN 1028-8546

2014, Vol. XX, № 3
Section: En

CONTENTS